Engineering Supermodes of Coupled Resonator Arrays

A Thesis Presented

by

Ruopeng Jia

to

The Department of Electrical and Computer Engineering

in partial fulfillment of the requirements

for the degree of

Master of Science

in

Electrical and Computer Engineering

Northeastern University

Boston, Massachusetts

April 2024

To my family.

List of Figures

1.1 A ring resonator and its transmission spectrum at the drop and through ports. . . . 2
1.2 A coupled-ring resonator chain with 10 rings, and its transmission spectrum at the drop port. . . . 3
1.3 Fourier transform and inverse-design based techniques to engineered spectrum of single-ring resonators. . . . 3

2.1 Schematic of a Ring Resonator and light propagations . . . 8
2.2 Transmission spectrum of a ring resonator at the drop and through ports. . . . 10
2.3 Schematic of a ring resonator structure showing two pseudospins and a structure designed to induce back-scattering effects and couple two pseudospins. . . . 11

3.1 Schematic of a system of two coupled resonators. . . . 13
3.2 Schematic of a 1D chain of resonators. . . . 15
3.3 Eigenfunctions and eigenvalues for a 1D chain of resonators. . . . 16
3.4 Schematic of a 1D chain with periodic boundary conditions. . . . 16
3.5 Eigenvalues and eigenfunctions for a super-ring - a 1D chain with periodic boundary conditions. . . . 18
3.6 Schematic of a 2D array of ring resonators and the labeling scheme. . . . 19
3.7 Eigenvalues and eigenfunctions for the 2D square lattice of ring resonators. . . . 20
3.8 Schematic of the topological 2D array of ring resonators with a synthetic magnetic field. The hopping phases are shown for two plaquettes. . . . 20
3.9 Eigenvalues and eigenfunctions for the topological 2D lattice simulating the integer quantum Hall model for photons, showing edge and bulk bands and their corresponding eigenfunctions. . . . 22
3.10 Robustness of edge states . . . 22

4.1 a. Schematic of a 1D resonator chain with OBC and modulated ring resonance frequencies. An example modulation pattern is shown in b. . . . 25
4.2 1D chain of 40 resonators with OBC: modulation pattern, a comparison of original and modulated eigenvalues, and the intensity pattern before and after modulation. . 26
4.3 1D chain of 40 resonators with OBC: modulation pattern as a sum of two frequencies, a comparison of original and modulated eigenvalues, and the intensity pattern before and after modulation. . . . 27

4.4 1D chain of 40 resonators with PBC: modulation pattern as a single frequency, a comparison of original and modulated eigenvalues, and the intensity pattern before and after modulation. 29
4.5 1D chain of 40 resonators with PBC: modulation pattern as a sum of two frequencies, a comparison of original and modulated eigenvalues, and the intensity pattern before and after modulation. 30
4.6 Engineering edge modes of the topological 2D resonator array using back-scattering. 31

5.1 The specific Genetic Algorithm process in Ring Resonator Array Optimization. . . 34
5.2 Optimization of a 40-ring 1D array with OBC where one pair of modes are shifted. We choose $\delta W = 0.2$, $f = 8$, and $\gamma_i = 1.0$ for all modes. a) The eigenvalues before any modulation. b) The desired shifts δE in supermode eigenvalues, c)the shifts achieved after FT, and d) the shifts after GO. e) The shifts in ring resonance frequencies from the sinusoidal modulation and f) after GO. 36
5.3 Optimization of a 40-ring 1D array with OBC where two pairs of modes are shifted. We choose $\delta W_1 = \delta W_2 = 0.2$, $f_1 = 8$, $f_2 = 14$ and $\gamma_i = 1.0$ for all modes. a) The eigenvalues before any modulation. b) The desired shifts δE in supermode eigenvalues, c)the shifts achieved after FT, and d) the shifts after GO. e) The shifts in ring resonance frequencies from the sinusoidal modulation and f) after GO. 37
5.4 Optimization of a 40-ring 1D array with OBC where only one mode is shifted. We choose $\delta W_1 = 0.2$, $f = 8$, and $\gamma_i = 1.0$ for all modes. a) The eigenvalues before any modulation. b) The desired shifts δE in supermode eigenvalues, c)the shifts achieved after FT, and d) the shifts after GO. e) The shifts in ring resonance frequencies from the sinusoidal modulation and f) after GO. 39
5.5 Optimization of a 40-ring 1D array with OBC where two modes, from different pairs, are shifted. We choose $\delta W_1 = \delta W_2 = 0.2$, $f_1 = 8$, $f_2 = 14$ and $\gamma_i = 1.0$ for all modes. b) The desired shifts δE in supermode eigenvalues, c)the shifts achieved after FT, and d) the shifts after GO. e) The shifts in ring resonance frequencies from the sinusoidal modulation and f) after GO. 40
5.6 Optimization of a 40-ring 1D array with OBC, where three modes, all from different pairs are shifted. a) The desired shifts δE in supermode eigenvalues, b) the shifts achieved after GO. c) The shifts in ring resonance frequencies from the sinusoidal modulation and after GO. d) Intensities of the 14^{th} (one of the shifted modes) mode after GO. 41
5.7 Optimization of a 40-ring 1D array with PBC, where two sets of modes, 8, 9, 32, and 33 are shifted. We choose $\delta W = 0.2$, $f = 8$, and $\gamma_i = 1.0$ for all modes. a) The eigenvalues before any modulation. b) The desired shifts δE in supermode eigenvalues, c)the shifts achieved after FT, and d) the shifts after GO. e) The shifts in ring resonance frequencies from the sinusoidal modulation and f) after GO. 43
5.8 Optimization of a 40-ring 1D array with PBC, where only one set of modes, 8, 9, are shifted. We choose $\delta W = 0.2$, $f = 8$, and $\gamma_i = 1.0$ for all modes. a) Original eigenvalues, b) the desired shifts δE in supermode eigenvalues, c) the shifts achieved after FT, and d) the shifts after GO. GO is not able to achieve the desired eigenmode spectrum. 44

6.1 SFWM in a ring resonator. The signal and idler photon pairs are generated in modes located symmetrically around the pumped mode. Joint spectral intensity (JSI) calculated for a single-ring resonator showing energy-time entanglement between the generated signal and idler photons. 47
6.2 JSD for a 1D resonator chain with PBC, with and without modulations. 48

7.1 Disorder compensation for a 1D resonator chain, with OBC, using genetic optimization. 53

List of Acronyms

SMA Single Mode Approximation.

ADF Add-Drop Filter.

FDTD Finite-Difference Time-Domain.

CW Clockwise.

CCW Counter-Clockwise.

OBC Open Boundary Condition.

PBC Periodic Boundary Condition.

GA Genetic Algorithm.

GO Genetic Optimization.

Acknowledgments

After a whole year, I still vividly recall the scene when I entered my advisor's office to apply for participation in this program. This journey has brought me fascinating experiences in physics and quantum mechanics, as well as a much deeper interest in the optical industries.

First and foremost, I would like to express my deepest appreciation to my advisor, Prof. Sunil Mittal. From his initial course, 'Introduction to Quantum Engineering', I was captivated by his in-class teaching style and understanding. Throughout my college experience, I have never encountered a better teacher. This course ignited my interest in quantum physics. Throughout the year, he has consistently been prepared for any conversation with me. His rigor, erudition, and insight have always motivated me to improve myself. Matching his academic standards was never easy, but the continuous progress has been rewarding. Despite his academic rigor, he is very approachable in daily life. We could discuss my future career, industry anecdotes, and daily routines without any limits. Additionally, I extend my gratitude to my defense committee members, Prof. Yongmin Liu and Prof. Siddhartha Ghosh, for providing invaluable suggestions and insights about the thesis. I would also like to thank my seniors, Seyed Danial Hashemi and Ankit Maisuriya, and Dr. Lin Deng for their enlightening discussions.

I would also like to express my gratitude to my roommates and friends, both near and far. It has been a challenging year, both mentally and physically, but my friends have always been there for me regardless of how things have changed. I am thankful to Yinghua for her enduring support over this extended period. Pursuing my dreams has never been easy, especially juggling two at the same time. I am particularly grateful to Yinghua, whose major in Ph.D. is history. I hope this expression of gratitude inspires her academically and accompanies her throughout her life. The greatest thanks are reserved for my parents, Xin Wang and Yongzheng Jia, for sustaining and encouraging me for over 24 years. Since childhood, I have been afforded the freedom to pursue my passions, a freedom that has remained unchanged. We have celebrated and overcome numerous challenges together as a family, of which I am immensely proud. I extend many thanks to Beethoven, Brahms, and Mendelssohn for their sublime melodies, which have helped me navigate through life.

I am grateful for all the insights and personal growth I have experienced in the past year and look forward to utilizing this harvest to explore further and never cease learning.

Abstract of the Thesis

Engineering Supermodes of Coupled Resonator Arrays

by

Ruopeng Jia

Master of Science in Electrical and Computer Engineering

Northeastern University, April 2024

Dr. Sunil Mittal, Advisor

Resonators form one of the most commonly used components of optical and on-chip photonic circuits and devices. Specifically, ring resonators, have enabled several on-chip photonic applications such as optical wavelength-multiplexed transmitters and receivers, optical wavelength filters, optical frequency combs, sensors, quantum light sources, and so on. Nevertheless, single resonators offer only a single degree of freedom, in the form of their longitudinal modes, to engineer the propagation of photons. Arrays of coupled resonators, where photons can hop from one resonator to its neighbors, provide an additional degree of freedom in the form of the supermodes of the array. Such coupled-resonator systems have been recently used, for example, to implement topological edge states, to engineer quantum light sources, and nested optical frequency combs.

In this thesis, we explore supermodes of different geometries of coupled resonator arrays, for example, one-dimensional and two-dimensional arrays, with different boundary conditions (open and closed), and their applications, for example, to generate quantum light. We use the simplified single-mode approximation that is valid when the coupling strength between the resonators is smaller than the free spectral range of the resonators. Using this formalism, we show that the supermode spectra are constrained by the inherent dispersion and symmetries of the array. Our results could lead to a better understanding of supermodes for applications in quantum light sources and optical frequency combs.

Chapter 1

Introduction

Integrated photonic ring resonators are one of the basic building blocks of integrated photonic devices and circuits. They enable a number of applications, such as intensity modulation for long-distance fiber-optic communication links and chip-scale communications between electronic circuits [1, 2, 3], sensors [4], wavelength filters, etc. More recently, ring resonators have also been used to implement neuromorphic computing architectures. The addition of optical nonlinearities in ring resonators, for example, the Kerr effect, opens the route to a host of other application domains such as the on-chip generation of optical frequency combs that find applications in spectroscopy, precision time-keeping, LiDARs, wavelength-multiplexed transmitters, and so on [5, 6, 7, 8]. Nonlinear ring resonators also provide an opportunity to generate quantum light, for example, entangled photon pairs on a chip [9, 10, 11].

Nevertheless, single-ring resonators offer only a single degree of freedom to control the propagation of photons, in the form of their longitudinal modes (resonances). This inherent limitation of single-ring resonators can be overcome using coupled-resonator systems that provide an additional degree of freedom, the longitudinal modes of coupled resonators, to engineer and control the flow of light [12, 13, 14]. The resonators are evanescently coupled meaning that photons can hop from one resonator to the neighboring resonators. Indeed, many such coupled-resonator systems have been demonstrated in the last decade or so, including one-dimensional arrays of ring resonators to implement on-chip optical delay lines [15, 16, 17] and flat-top bandpass filters [18], quantum light sources [19, 20]. More recently, two-dimensional arrays of coupled-ring resonators have been used to demonstrate the intriguing physics of topological edge states that are remarkably robust against fabrication disorders, such as random variations in ring resonance frequencies or even a missing ring resonator [21, 22, 23]. Such topological ring resonator arrays have also been used to implement

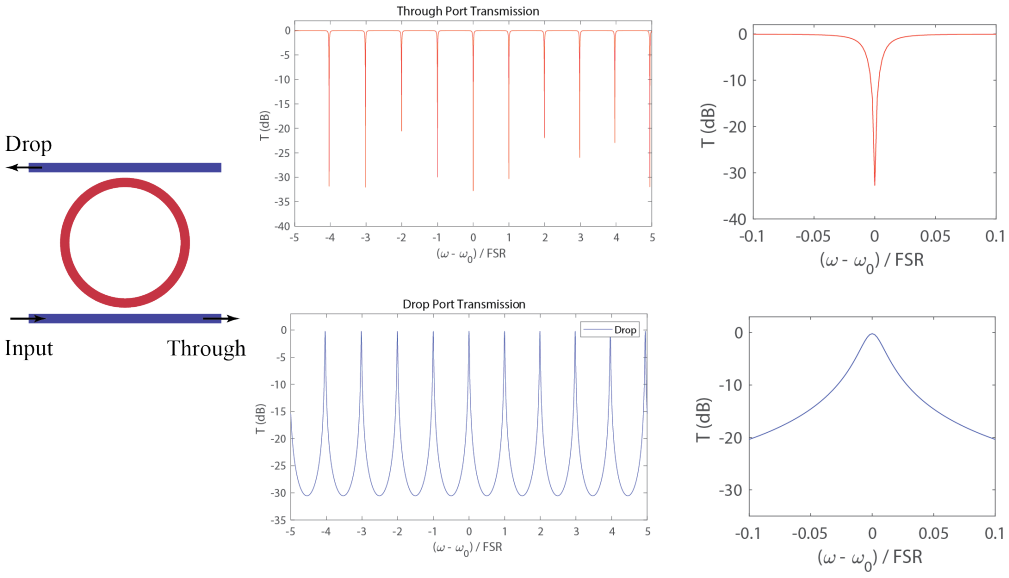


Figure 1.1: A ring resonator and its transmission spectrum at the drop and through ports.

robust, spectrally-engineered tunable quantum light sources [24, 25, 26], and novel nested optical frequency combs [27].

A common challenge with coupled resonator arrays is the control over the supermode structure, that is, the control over the frequencies where the supermode resonances appear. Usually, coupled-resonator systems employ periodic 1D or 2D arrays. The supermode structure in these periodic systems is governed by the lattice geometry, for example, the dimensions (1D or 2D) of the array, the boundary conditions which could be open or periodic (open), the number of different resonators that constitute a unit cell of the lattice, the underlying symmetries of the array, inclusion of synthetic gauge fields, and so on.

In this thesis, we explore inverse-design techniques to spectrally engineer a specific supermode or a set of supermodes of this otherwise uniform 1D or 2D resonator arrays. The goal of this engineering will be to selectively shift the resonance frequency of a single or a pair of target supermodes while fixing the resonance frequencies of all other supermodes. While we specifically target ring resonators, our results are applicable to other coupled-resonator systems, for example, those implemented using photonic crystal cavities.

The techniques that we use to engineer the supermodes of coupled resonator arrays are inspired by some very recent demonstrations of engineering the uniformly-spaced (in the absence of dispersion) longitudinal modes of a single-ring resonator [28, 29]. For example, in Figure 1.3

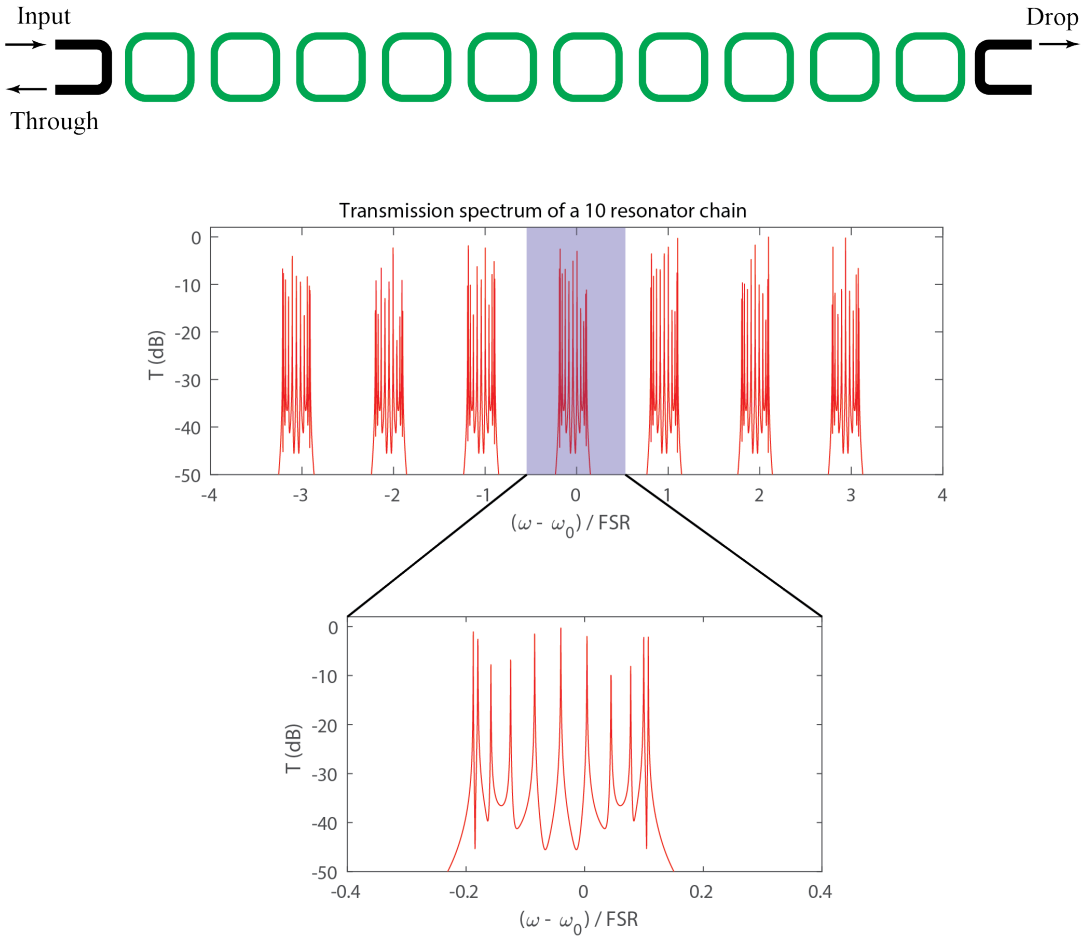


Figure 1.2: A coupled-ring resonator chain with 10 rings, and its transmission spectrum at the drop port.

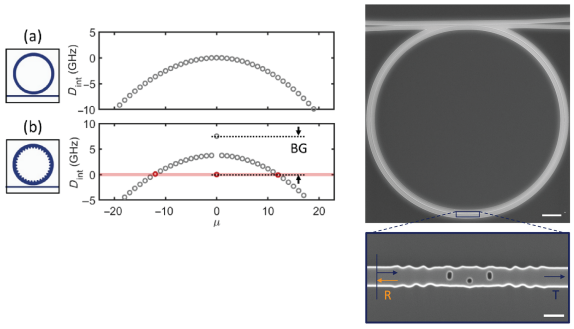


Figure 1.3: Fourier transform and inverse-design based techniques to engineered spectrum of single-ring resonators.

we show a single-ring resonator whose width undergoes a sinusoidal modulation pattern with a given frequency. This modulation pattern couples the clockwise (CW) and counter-clockwise (CCW) circulating modes in the ring via back-scattering, and thereby, breaks the degeneracy of their resonance frequencies and splits them. More importantly, the use of a sinusoidal pattern ensures that the resonance frequencies of only a single longitudinal mode, whose phase distribution in the ring coincides with the frequency of the modulation pattern, are shifted. This scheme can be extended to include combinations of different frequencies that shift a set of target supermodes. This scheme has been recently used to increase the efficiency of single-ring resonator-based optical frequency combs. We will refer to such schemes that use periodic modulation patterns as Fourier transform-based techniques.

Another inverse-design approach that has been demonstrated very recently uses an array of holes in the ring resonator waveguides to achieve a target longitudinal mode structure [30]. The sizes of the holes and their positions are calculated using a combination of Finite-Difference Time-Domain (FDTD) and inverse-design approaches. Nevertheless, the underlying mechanism of engineering the longitudinal mode structure is the same - the holes couple CW and CCW modes of the ring resonator via back-scattering and the strength of this coupling controls the splitting between the resonance frequencies. The main advantage of this technique, over the Fourier transform technique, is that the coupling strength, and hence the splitting, can be designed to be different for different longitudinal modes.

The central theme of the thesis is to use these inverse-design techniques to engineer the supermodes of coupled-ring resonator arrays. The periodic modulation or the addition of holes in the ring resonator waveguides (for a single-ring resonator) are emulated in the coupled-ring resonator structure by modulating the resonance frequencies of the rings. We emphasize that, throughout this thesis, the waveguides of individual ring resonators will not be modulated. For example, there will not be any back-scattering-induced coupling between the CW and CCW modes of individual ring resonators. Instead, we will couple the CW and CCW supermodes that propagate around the resonator array. In principle, it is possible to modulate both, the individual ring resonator waveguides as well as the ring resonance frequencies, and achieve a much more complex simultaneous engineering of both the longitudinal modes of the individual rings and the supermodes of the array. Such engineering is outside the scope of this thesis. Furthermore, all results presented in this thesis are numerical simulation results, but our approach can be easily demonstrated in experiments, for example, using silicon or silicon-nitride ring resonators.

The thesis is organized as follows:

In Chapter 2, we will detail the single-mode approximation that we will use to describe a single-ring resonator near one of its longitudinal mode frequencies. As the name suggests, this is an approximation that treats the ring resonator as a single lumped element and ignores any variation of light intensity along the ring resonator. This approximation is valid as long as the losses in the ring are small compared to its free-spectral range, which is indeed the case for many applications of ring resonators.

In Chapter 3, we will use the single-mode approximation, also referred to as the coupled-mode theory, to describe coupled resonator arrays. Using this approach, we will write a Hamiltonian matrix for the array. The eigenvalues and eigenvectors of this Hamiltonian matrix will yield the resonance frequencies of the supermodes and their intensity profiles (or wavefunctions) in the array. The supermode wavefunctions will provide useful information about the nature of supermodes, for example, if they are traveling or standing-wave resonances, the phase they accumulate in the array, the rings they occupy, their symmetries, and so on. We will specifically discuss 1D resonator chains with open-boundary conditions, periodic boundary conditions, with synthetic gauge fields, 2D resonator arrays on a square lattice, and 2D resonator arrays with synthetic gauge fields that exhibit topological edge states.

In Chapter 4, we will show examples of Fourier transform techniques to engineer the supermodes of arrays. Similar to single-ring resonators, we will use sinusoidal modulation (time-independent) of ring resonance frequencies, that is, different rings in the array will have specifically chosen resonance frequencies. We will demonstrate supermode engineering of 1D resonator chains with open and periodic boundary conditions. We find that the discrete nature of the resonator array prevents a very selective shift of a single supermode and it marginally shifts the resonance frequencies of neighboring supermodes. We will also discuss this engineering in the context of 2D topological arrays and find that this simple scheme fails because of the inherent robustness of edge states. We used another scheme that couples CW and CCW modes within each ring resonator, but we found that even this scheme is not able to selectively shift a single topological supermode.

In Chapter 5, we will use a combination of Fourier transform and genetic optimization (GO) techniques to improve supermode engineering. Specifically, we will use GO to reduce the unintended shifts in resonance frequencies of neighboring supermodes that appear when using Fourier transform techniques to engineer a given supermode.

In Chapter 6, we will discuss a coupled-resonator quantum source of entangled photon pairs that uses selective engineering of the supermodes to control the spectral-temporal correlations/entanglement between photon pairs.

In Chapter 7, we will present opportunities for more complex spectral engineering of coupled resonator arrays that could enable spectrally-engineered nested optical frequency combs and quantum light sources.

Chapter 2

Ring Resonators

Ring resonators find a number of applications in photonic integrated circuits, in the form of modulators, optical-add-drop multiplexers, filters, sensors, and so on. At the most fundamental level, a ring resonator is a waveguide folded onto itself (see Figure 2.1). This folding leads to interference effects such that only the frequencies satisfying the relation

$$\frac{\omega}{c}\, n_{eff}\, L = \; k\, L = \; m\, 2\pi \tag{2.1}$$

undergo constructive interference and survive in the ring. Here, ω is the angular frequency of light, n_{eff} is the effective refractive index of the waveguide at the frequency ω, L is the total length of the resonator, and m is an integer. Therefore, $k\, L$ is the total phase accumulated in the ring resonator, with $k = \frac{\omega}{c}\, n_{eff}$ being the propagation constant. The ring resonator exhibits a resonance, meaning an increase in light intensity contained in the ring, at each frequency ω that satisfies the above relation. We label these resonance frequencies using $\omega_m = \frac{m\, 2\pi\, c}{n_{eff}\, L}$. The modes corresponding to these resonance frequencies are referred to as the longitudinal modes. A mode indexed by label m accumulates a total phase of $m2\pi$ around the ring resonator.

The angular frequency spacing between the modes is called the free-spectral range (FSR, Ω) and can be calculated as

$$\Omega = \frac{2\pi\, c}{n_g\, L} = \frac{2\pi\, v_g}{L}. \tag{2.2}$$

Here, n_g is the group index and it takes into account the variation of the refractive index as a function of frequency. $v_g = \frac{c}{n_g}$ is the group velocity. The round-trip time τ_r, which is the time it would take for a pulse to travel around the ring, is related to FSR Ω as

$$\tau_r = \frac{L}{v_g} = \frac{2\pi}{\Omega}. \tag{2.3}$$

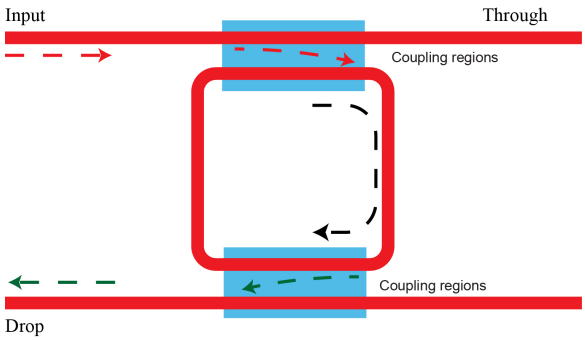


Figure 2.1: Schematic of a Ring Resonator and light propagations

2.1 Input-Output Coupling and Single-Mode Approximation

To inject light in and out of the ring resonator, the resonator is usually placed in close proximity to one or two straight waveguide sections as shown in Figure 2.1. The waveguides are evanescently coupled to the ring resonator meaning that light traveling in the straight waveguide (injected from the input port) can leak into the ring resonator. Similarly, light traveling in the ring resonator waveguide can couple back into the input waveguide or the output waveguide. Figure 2.1 shows the ring coupled to two waveguides - a geometry referred to as the add-drop filter with four ports. If light is injected at the input port and its angular frequency is close to one of the resonance frequencies, light couples to the ring and appears at the drop port. If the frequency of the incoming light is far away from the resonance frequency, the light does not couple to the ring resonator and it appears on the through port.

For a given frequency, the fraction of input light intensity that appears at the drop/through ports, and the intensity of light in the ring resonator can be calculated using the single-mode approximation (SMA) [1]. This approximation is valid when the total loss of the ring resonator, that is, the extrinsic loss to input/output waveguides and the intrinsic loss due to any absorption or scattering from ring waveguides is small. Furthermore, this approximation represents the dynamics of the ring resonator only near one of the resonance frequencies (indicated as ω_0).

In this approximation, we represent the ring as a lumped element with energy amplitude a, which is related to the power $|\mathcal{E}|^2$ as

$$|a|^2 \frac{v_g}{L} = |\mathcal{E}|^2. \tag{2.4}$$

The equation that describes the evolution of the amplitude a is given as [1]

$$\frac{da}{dt} = -i\,\omega_0\,a - (2\kappa_{ex} + \kappa_{in})\;a + i\,\sqrt{2\kappa_{ex}}\,\mathcal{E}_{in}\,e^{-i\,\omega\,t}. \tag{2.5}$$

Here ω_0 is the resonance frequency for a given mode. κ_{ex} is the loss to input/output waveguides and is referred to as the extrinsic loss. κ_{in} is the intrinsic loss due to absorption or scattering. We included a factor of 2 in the extrinsic loss κ_{ex} to account for loss to the two input/output waveguides (add-drop filter geometry). $\mathcal{E}_{in}$ is the input electric field amplitude such that $|\mathcal{E}_{in}|^2$ is the input power. The angular frequency of the incoming field is ω.

Using a solution of the type $a = ae^{-i\,\omega\,t}$ in the above equation, the steady-state solution for the amplitude a in the ring resonator can be calculated as

$$a = \frac{\sqrt{2\,\kappa_{ex}}\,\mathcal{E}_{in}}{-i\,(\omega-\omega_0)+(2\kappa_{ex}+\kappa_{in})}. \tag{2.6}$$

The total energy in the ring resonator is calculated as

$$|a|^2 = |\mathcal{E}_{in}|^2 \frac{2\,\kappa_{ex}}{(\omega-\omega_0)^2+(2\kappa_{ex}+\kappa_{in})^2}. \tag{2.7}$$

The energy in the ring is maximum when the incoming light frequency ω coincides with the ring resonance frequency ω_0.

The electric field amplitude $\mathcal{E}_D$ at the drop port is related to a as

$$\mathcal{E}_D \;=\; i\,\sqrt{2\,\kappa_{ex}}\,a \;=\; \frac{-2\,\kappa_{ex}\,\mathcal{E}_{in}}{-i\,(\omega-\omega_0)+(2\kappa_{ex}+\kappa_{in})}. \tag{2.8}$$

Similarly, the electric field amplitude $\mathcal{E}_T$ at the through port is

$$\mathcal{E}_T \;=\; \mathcal{E}_{in} + i\,\sqrt{2\,\kappa_{ex}}\,a \;=\; \mathcal{E}_{in}\frac{-i\,(\omega-\omega_0)+\kappa_{in}}{-i\,(\omega-\omega_0)+(2\kappa_{ex}+\kappa_{in})}. \tag{2.9}$$

Using these equations, we can write the output powers at the drop and through ports as

$$P_D \;=\; |\mathcal{E}_D|^2 = P_{in}\frac{4\kappa_{ex}^2}{(\omega-\omega_0)^2+(2\kappa_{ex}+\kappa_{in})^2} \tag{2.10}$$

$$P_T \;=\; |\mathcal{E}_T|^2 = P_{in}\frac{(\omega-\omega_0)^2+\kappa_{in}^2}{(\omega-\omega_0)^2+(2\kappa_{ex}+\kappa_{in})^2} \tag{2.11}$$

$$\tag{2.12}$$

We find that at resonance, that is, $\omega = \omega_0$, and for $\kappa_{in} = 0$, $\mathcal{E}_D = \mathcal{E}_{in}$ and $\mathcal{E}_T = 0$. As mentioned earlier, at resonance, the output at the through port is zero and all light intensity appears at the drop port. For a finite loss, $\kappa_{in} \neq 0$, the output at the drop port reduces, and that at the through port increases.

Figure 2.2 shows a typical transmission spectrum for the ring resonator at both the drop and the through ports, calculated using $\kappa_{ex} = 1$ and $\kappa_{in} = 0.1$. We find that, because of the finite loss of

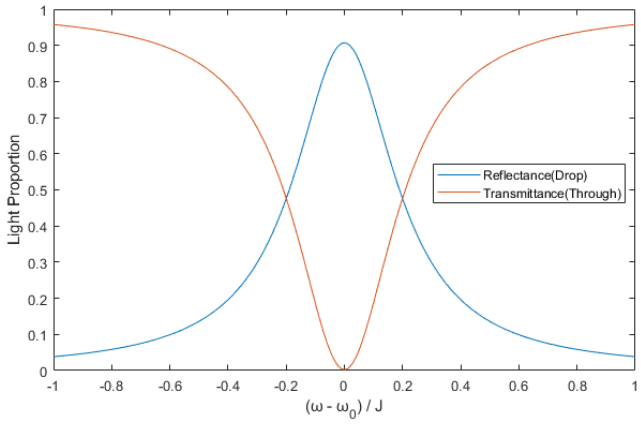


Figure 2.2: Transmission spectrum of a ring resonator at the drop and through ports.

the ring resonator, light of frequency close to the ring resonance frequency ω_0 can have appreciable intensity in the ring resonator. The bandwidth of the transmission spectrum can be calculated as $2\left(2\kappa_{ex} + \kappa_{in}\right)$. We emphasize that the ring exhibits a similar transmission spectrum at each of its resonance frequencies ω_m. The above SMA analysis holds nearly only one of these resonances. In this thesis, we will exclusively use the single-mode approximation when we discuss the modes of the coupled resonator arrays.

2.2 Pseudospins in a Ring Resonator

A ring resonator supports two directions of circulation in the ring, clockwise (CW) and counter-clockwise (CCW) (Figure 2.3). We will refer to them as two pseudospins. We can excite either pseudospin by appropriately choosing the input port. For example, in Figure 2.1, we light is injected at the input port, it will excite the CW propagating pseudospin in the ring. In contrast, if light is injected from the drop port, it will excite the CCW pseudospin in the ring.

In the absence of any back-scattering from the ring waveguides, the two pseudospins are decoupled from each other meaning that exciting one of the pseudospins does not excite the other pseudospin. Furthermore, the two pseudospins are time-reversed pairs and they exhibit the same resonance frequencies because they both acquire the same phase in the ring resonator.

Nevertheless, any unintentional back-scattering in the waveguides or specially designed structures to induce back-scattering (Figure 2.3 .b) will couple the two spins. This coupling will break the degeneracy between the two pseudospins and it will create a frequency splitting between

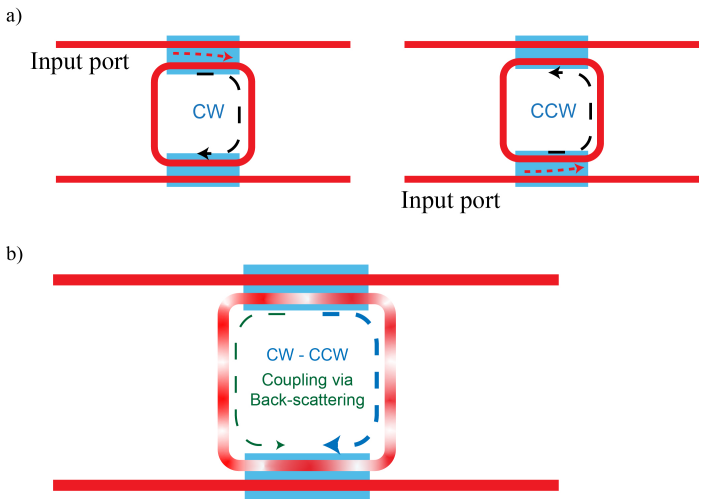


Figure 2.3: Schematic of a ring resonator structure showing two pseudospins and a structure designed to induce back-scattering effects and couple two pseudospins.

the two eigenmodes of the ring. We will discuss this frequency splitting in the next chapter.

Chapter 3

Coupled Ring Resonator Arrays

As we discussed in the last chapter, a ring resonator supports multiple longitudinal modes, exactly one mode at each at its resonance frequencies ω_m. By coupling multiple resonators together, for example, in the form of 1D or 2D lattices, we can achieve a number of supermodes around each resonance frequency ω_m. These supermodes provide an additional degree of freedom to control the photonic spectral mode structure. Only very recently, these supermodes have been used, for example, to implement high-order on-chip spectral filters, implement topologically robust phases of light, realize topologically robust lasers, generate quantum states of light with engineered spectral-temporal correlations, for generating nested optical frequency combs, etc. In this chapter, we will discuss the tight-binding Hamiltonian formalism that we will use to describe such coupled-resonator systems and the properties of their supermodes.

3.1 Hamiltonian formalism for a photonic molecule

To understand the Hamiltonian description of coupled resonator systems, we will first describe a photonic molecule, that is, a system of two resonators that are coupled together using evanescent field coupling (see Figure 3.1). For simplicity, we will assume that the two rings are identical and have the same resonance frequency ω_0. This system can be described using the Hamiltonian

$$H = \omega_0 a_1^\dagger a_1 + \omega_0 a_2^\dagger a_2 - J a_2^\dagger a_1 - J a_1^\dagger a_2. \tag{3.1}$$

Here, a_1 and a_2 are the annihilation operators for photons in the first and second rings, respectively. $a_1^\dagger$ and $a_2^\dagger$ are the corresponding creation operators. The first two terms represent the self-energy of the two ring resonators, and the last two terms represent the hopping of photons between the two

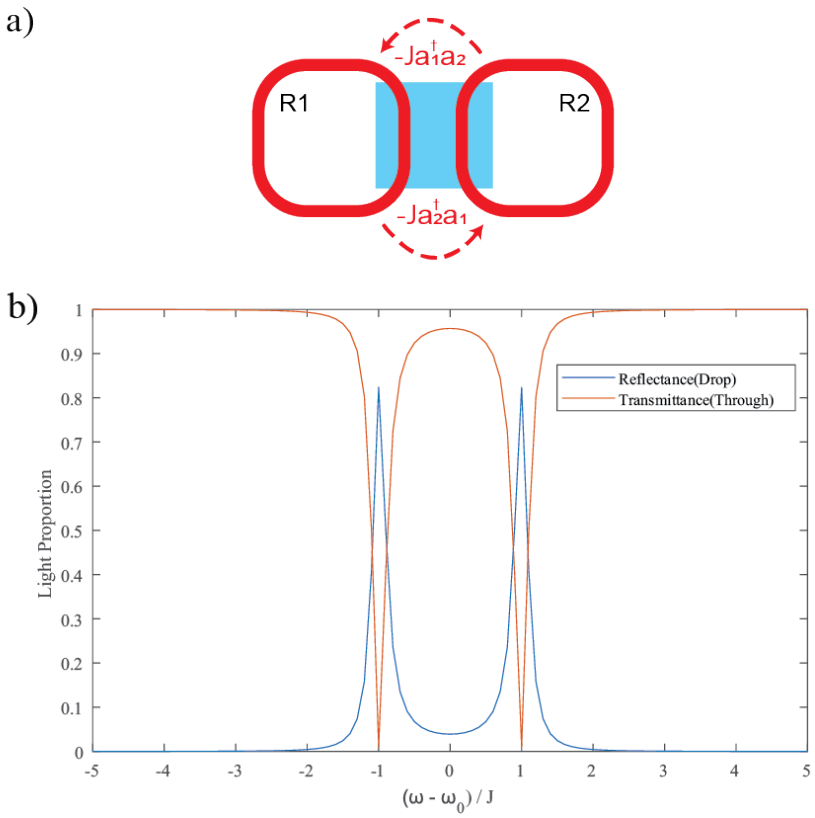


Figure 3.1: Schematic of a system of two coupled resonators.

resonators. Here J is the strength of coupling between the resonators such that the coupling strength increases when the two resonators are brought together.

This Hamiltonian can be expressed in the matrix form as

$$H = \begin{pmatrix} a_1^\dagger & a_2^\dagger \end{pmatrix} \begin{pmatrix} \omega_0 & -J \\ -J & \omega_0 \end{pmatrix} \begin{pmatrix} a_1 \\ a_2 \end{pmatrix}. \tag{3.2}$$

The two eigenvalues of this 2×2 Hamiltonian matrix can be calculated to be $\omega_+ = \omega_0 + J$ and $\omega_- = \omega_0 - J$. Thus, we find that the eigenvalues of two ring resonators, originally with the same resonance frequencies, have split into a pair of resonances with a frequency difference $2J$.

The corresponding eigenfunctions of this Hamiltonian can be calculated as

$$|\psi\rangle_- = \frac{1}{\sqrt{2}} \begin{pmatrix} 1 \\ 1 \end{pmatrix}, \quad |\psi\rangle_+ = \frac{1}{\sqrt{2}} \begin{pmatrix} 1 \\ -1 \end{pmatrix}. \tag{3.3}$$

The eigenfunction $|\psi\rangle_-$, with corresponding eigenvalue ω_-, is the symmetric combination of both resonator modes. Similarly, the eigenfunction $|\psi\rangle_+$, with corresponding eigenvalue ω_+, is the anti-symmetric combination of both resonator modes.

3.2 Coupling of Two Pseudo-Spins in a Ring Resonator

As we discussed in Chapter 2, a ring resonator supports two pseudospins which are the modes circulating around the ring in CW and CCW directions. These two pseudospins are decoupled and degenerate in their resonance frequency in the absence of any back-scattering. Any coupling (intentional or unintentional) will couple the two pseudospins and lift this degeneracy. In this section, we will describe this coupling using the Hamiltonian formalism we used for a photonic molecule.

We will begin by representing the CW and CCW circulating modes with corresponding amplitudes a_{CW} and a_{CCW}. The Hamiltonian is then written as

$$H = \omega_0 a_{CW}^\dagger a_{CW} + \omega_0 a_{CCW}^\dagger a_{CCW} - J a_{CCW}^\dagger a_{CW} - J a_{CW}^\dagger a_{CCW} \tag{3.4}$$

$$= \begin{pmatrix} a_{CW}^\dagger & a_{CCW}^\dagger \end{pmatrix} \begin{pmatrix} \omega_0 & -\beta \\ -\beta & \omega_0 \end{pmatrix} \begin{pmatrix} a_{CW} \\ a_{CCW} \end{pmatrix}. \tag{3.5}$$

Here, β is the coupling factor between the CW and CCW modes. Following our analysis of the photonic molecule, we can calculate the eigenfrequencies (or resonance frequencies) of the system as $\omega_\pm = \omega_0 \pm \beta$, and the corresponding eigenfunctions are symmetric and anti-symmetric combinations of CW and CCW propagating modes. We note that even exciting a single pseudospin from the input port will lead to the excitation of both the pseudospins in the ring resonator. In Chapter 4, We will use this coupling to engineer the modes of coupled resonator systems.

3.3 1D Coupled-Resonator Chain

We will now discuss a 1D chain of coupled resonators as shown in Figure 3.2. For simplicity, here we will assume that all the ring resonators have the same resonance frequency ω_0. Furthermore, each ring is only coupled to its nearest neighbors, with the coupling strength J. The Hamiltonian describing this 1D chain of N resonators is written as

$$H = \sum_{n=1}^{N} \omega_0 a_n^\dagger a_n - J \sum_{n=1}^{N-1} a_{n+1}^\dagger a_n - J \sum_{n=1}^{N-1} a_n^\dagger a_{n+1}. \tag{3.6}$$

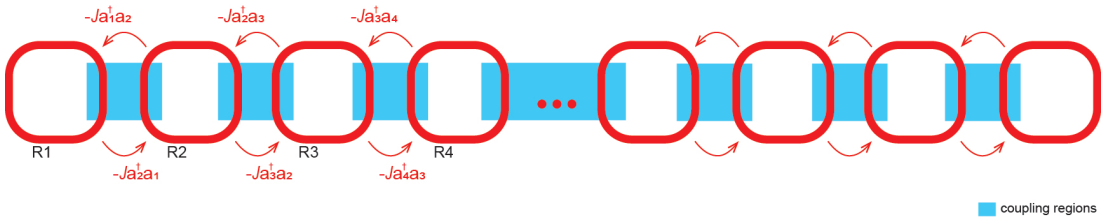


Figure 3.2: Schematic of a 1D chain of resonators.

Here, we have labeled the ring resonators from left to right as $n = 1$ to N (see Figure 3.1). As before, the first term $\omega_0 a_n^\dagger a_n$ represents the self-energy of the n^{th} resonator. The term $J a_{n+1}^\dagger a_n$ represents the hopping of photons towards the right. The term $J a_n^\dagger a_{n-1}$ represents the hopping of photons towards the left.

This Hamiltonian can be represented in the matrix form as

$$H = \begin{pmatrix} a_1^\dagger & a_2^\dagger & \dots & a_N^\dagger \end{pmatrix} \begin{pmatrix} \omega_0 & -J & 0 & \dots & 0 \\ -J & \omega_0 & -J & \dots & 0 \\ \vdots & & & & \\ \dots & 0 & 0 & -J & \omega_0 \end{pmatrix} \begin{pmatrix} a_1 \\ a_2 \\ \vdots \\ a_N \end{pmatrix}. \tag{3.7}$$

For a chain with N resonators, the dimension of the Hamiltonian matrix is $N \times N$, and accordingly, it exhibits N eigenvalues and N eigenvectors. The eigenvalues of this chain are the resonance frequencies of the supermodes of the chain, and the corresponding eigenfunctions are the longitudinal modes of the chain.

Figure 3.3 .a shows the calculated eigenvalues for a chain of 20 resonators. The eigenvalues are symmetric around ω_0 and follow the equation

$$\omega^{(n)} = \omega_0 + sin\left(\frac{(n - N/2)}{N}\pi\right). \tag{3.8}$$

Figure 3.3 .b-d show intensity distribution (calculated using the absolute square of the eigenfunctions) in the resonator chain for three different eigenvalues. We find that the intensity distribution in the chain follows a sinusoidal pattern. Furthermore, the frequency of oscillation of this pattern increases with the energy of the eigenfunction. This sinusoidal intensity distribution indicates that the supermodes of this 1D resonator chain are in fact the longitudinal modes of a standing-wave resonator similar to that of a stretched string.

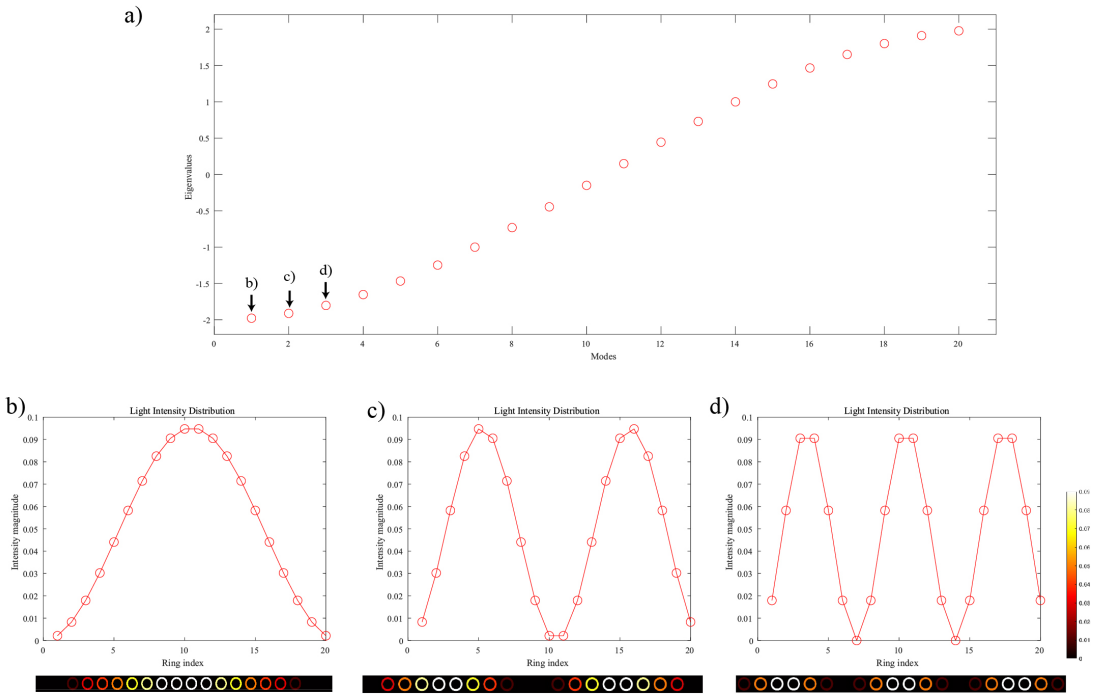


Figure 3.3: Eigenfunctions and eigenvalues for a 1D chain of resonators.

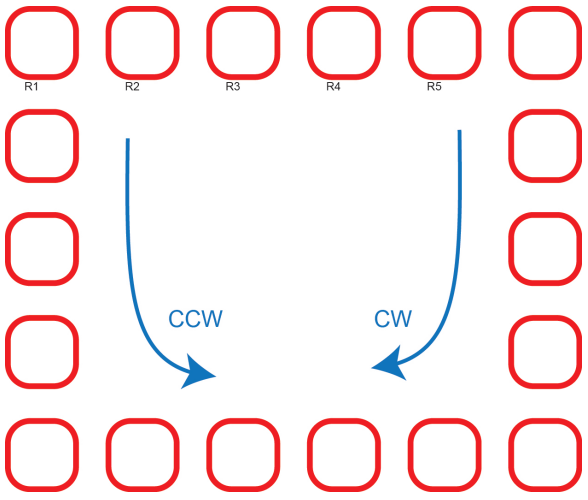


Figure 3.4: Schematic of a 1D chain with periodic boundary conditions.

3.4 1D Coupled-Resonator Super-Ring

Next, we discuss a super-ring made of ring resonators, that is, a 1D resonator chain with periodic boundary conditions (see Figure 3.4). We will see that changing the boundary condition changes the nature of the longitudinal modes of the array.

This periodic chain is described by a Hamiltonian

$$H = \sum_{n=1}^{N} \omega_0 a_n^\dagger a_n - J \sum_{n=1}^{N-1} a_{n+1}^\dagger a_n - J \sum_{n=1}^{N-1} a_n^\dagger a_{n+1} - J a_N^\dagger a_1 - J a_1^\dagger a_N. \tag{3.9}$$

which includes the hopping of photons between resonator 1 and N.

In Figure 3.5, we plot the calculated eigenvalues for this super-ring. We find that the eigenvalues are now doubly degenerate, that is, eigenvalues always appear in pairs (except the first and the last eigenvalues).

In Figure 3.5 .b and c, we plot the intensity distribution in the supermode for two different eigenfrequencies. We find that the intensity distribution in the super-ring is uniform. This is in contrast to the 1D resonator chain with open-boundary conditions where the intensity distribution exhibits a sinusoidal oscillating pattern. This clearly indicates that the supermodes of this super-ring structure correspond to the longitudinal modes of the super-ring that form traveling waves. Furthermore, the pair of degenerate eigenvalues correspond to waves traveling around the super-ring in clockwise (CW) and counter-clockwise (CCW) directions. This is evidenced by the phase that the eigenmodes acquire when propagating through one round-trip of the super-ring. For example, the second eigenmode (indicated in Figure 3.5 .b) acquires a phase of $+2\pi$ through the lattice. The third eigenmode in Figure 3.5 .c, which is degenerate with the second eigenmode, acquires a phase -2π through the lattice. We find that these longitudinal supermodes of the periodic 1D array behave in a very similar way to the longitudinal modes of a single-ring resonator, that is, they exhibit a two-fold degeneracy, the degenerate eigenstates circulate around the lattice in opposite directions, and the phase acquired by the supermodes is $\pm m\ 2\pi$. Therefore, we refer to this 1D array with periodic boundary conditions as a super-ring.

3.5 2D Resonator Arrays on a Square Lattice

In this section, we will discuss a 2D array of ring resonators arranged in the form of a square lattice (see Figure 3.6). We will label the rings using two indices (x, y) that are the locations of the ring along the $x-$axis and $y-$axis, respectively. As before, for simplicity, we will assume that

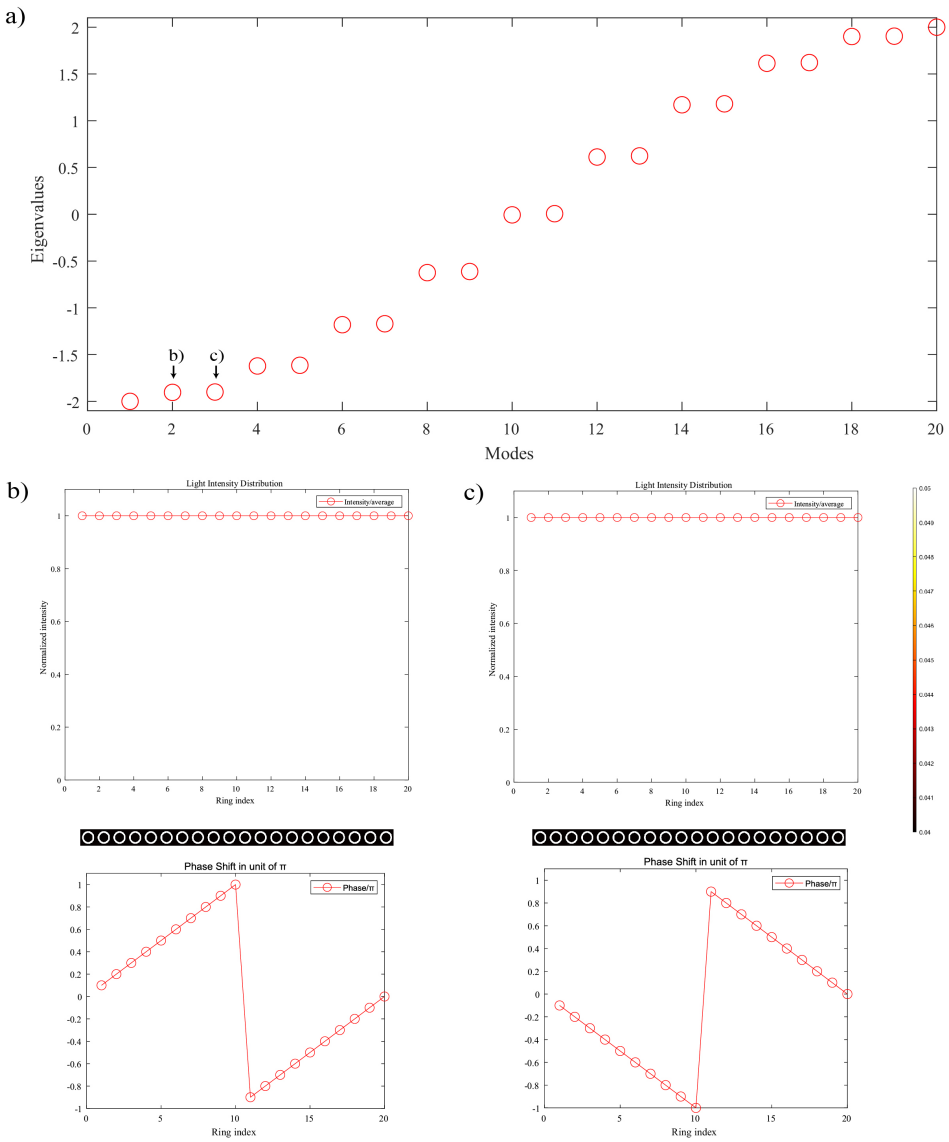


Figure 3.5: Eigenvalues and eigenfunctions for a super-ring - a 1D chain with periodic boundary conditions.

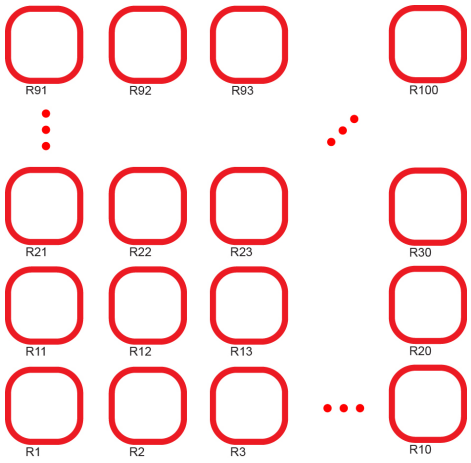


Figure 3.6: Schematic of a 2D array of ring resonators and the labeling scheme.

all the rings are the same with resonance frequency ω_0. Furthermore, the rings are coupled only to their nearest neighbors, both along the horizontal and the vertical directions, with coupling strength J.

The Hamiltonian for this 2D square lattice can be written as

$$H = \sum_{x=1}^{N_x} \sum_{y=1}^{N_y} \left[\omega_0 a_{x,y}^\dagger a_{x,y} - J a_{x,y+1}^\dagger a_{x,y} - J a_{x,y}^\dagger a_{x,y+1} - J a_{x+1,y}^\dagger a_{x,y} - J a_{x,y}^\dagger a_{x+1,y} \right] \quad (3.10)$$

Here, $a_{x,y}$ is the annihilation operator at a lattice site (m, n). The term $J a_{x,y+1}^\dagger a_{x,y}$ represents the hopping of photons along the $+$ve $y-$axis, the term $J a_{x+1,y}^\dagger a_{x,y}$ represents the hopping of photons along the $+$ve $x-$axis, and so on. N_x and N_y are the number of lattice sites along the $x-$axis and $y-$ axis, respectively. The total number of rings in the lattice is $N = N_x \times N_y$.

Accordingly, the Hamiltonian for this lattice is a matrix of dimension $N \times N$ and exhibits N eigenvalues and N eigenfunctions. Figure 3.7 .a shows the calculated eigenvalues for a 10×10 array, with $\omega_0 = 0$ and $J = 1$. Figure 3.7 .b shows the intensity distribution in the lattice for two eigenvalues as indicated in Figure 3.7 .a. We find that the eigenvalues are symmetric around ω_0 and they constitute a single band without any bandgaps.

3.6 Topological 2D Resonator Arrays with a Synthetic Magnetic Field

In this section we will discuss the introduction of a synthetic magnetic field in the 2D square lattice of ring resonators, and how it leads to the emergence of topologically robust edge

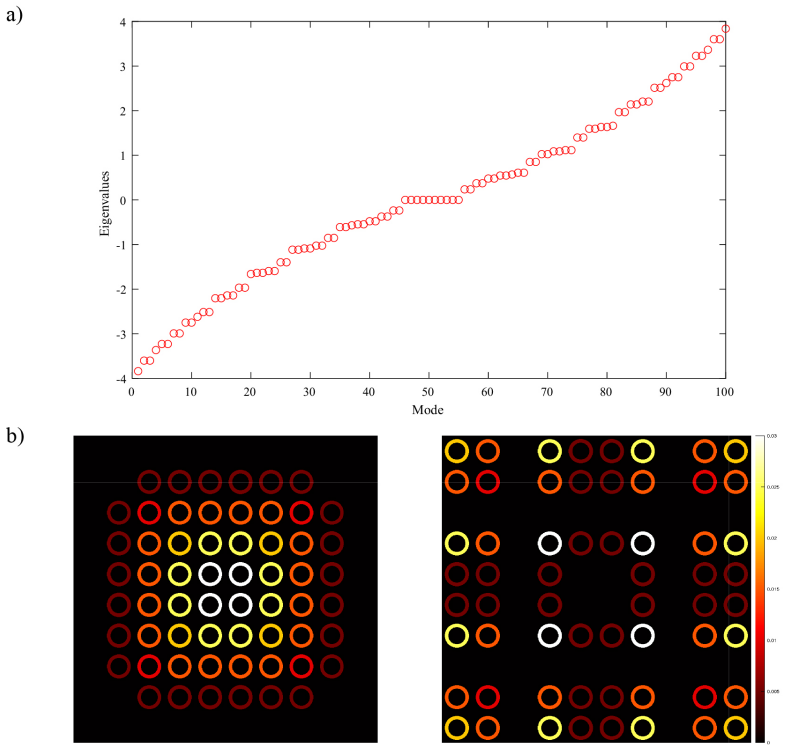


Figure 3.7: Eigenvalues and eigenfunctions for the 2D square lattice of ring resonators.

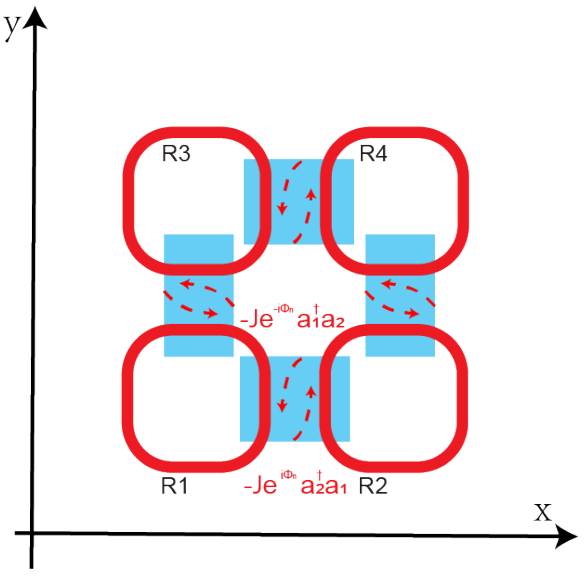


Figure 3.8: Schematic of the topological 2D array of ring resonators with a synthetic magnetic field. The hopping phases are shown for two plaquettes.

states. We will follow the model introduced in Refs. [21, 22] that implements the integer quantum Hall model for photons.

Specifically, in this model, the photons acquire a direction and position-dependent phase as they hop between the neighboring lattice site of the 2D array. This hopping phase is chosen to be $\phi_n = +2\pi\ \alpha\ n$ when the photons hop along the positive $x-$axis at the $y-$location n (see Figure 3.8). The hopping phase is $\phi_n = -2\pi\ \alpha\ n$ when the photons hop along the negative $x-$axis at the $y-$location n. The direction dependence of the hopping phase is evident in the sign of the hopping phase, and its position dependence is given by the $y-$location n. Here α is a number of the form $\frac{p}{q}$ where p and q are mutually prime integers.

This choice of hopping phases leads to an interesting scenario where the hopping phase is $+\phi = 2\pi\alpha$ whenever the photons hop in any plaquette (a unit of 4 lattice sites) of the lattice in the clockwise direction. But, the hopping phase is $-\phi = -2\pi\alpha$ when the photons hop around any plaquette in the counter-clockwise direction. It has been shown that this uniform hopping phase is equivalent to having a uniform synthetic magnetic field in the lattice and this photonic system simulates the integer quantum Hall model for electrons. This choice of hopping phases implements the Landau gauge with a magnetic field flux ϕ pointing perpendicular to the 2D lattice.

The Hamiltonian for this 2D system with a magnetic flux is written as

$$H = \sum_{x=1}^{N_x}\sum_{y=1}^{N_y}\left[\omega_0 a^\dagger_{x,y}a_{x,y} - Ja^\dagger_{x,y+1}a_{x,y} - Ja^\dagger_{x,y}a_{x,y+1} - Je^{i\phi_n}a^\dagger_{x+1,y}a_{x,y} - Je^{-i\phi_n}a^\dagger_{x,y}a_{x+1,y}\right] \tag{3.11}$$

Note that the hopping phase ϕ_n is included only for photons hopping along the $x-$axis, its magnitude is a function of the $y-$location n and its sign depends on the hopping direction along the $x-$axis.

Figure 3.9 shows the calculated eigenvalues for a 10×10 lattice of rings, with $\alpha = 1/4$ and $\phi = \pi/2$. We see the emergence of distinct bands as highlighted in the figure. In particular, we find two edge bands and four bulk bands. The intensity distribution corresponding to eigenvalues in the edge bands is confined to the edge (boundary) of the lattice (see Figure 3.9 .a). Furthermore, the eigenfunctions in the two edge bands are distinct as they propagate around the lattice in opposite directions (CW and CCW). Their circulation direction in the lattice can be inferred from the flow of their probability currents. In contrast to the states in the edge bands, the intensity distribution for states in the bulk bands is distributed in the bulk of the lattice.

The edge states are topologically protected against disorders, for example, in the ring resonance frequencies [31]. To show this disorder, in Figure 3.10, we plot calculated eigenvalues for 5 different realizations of the lattice with random disorders, with peak frequency shift $\delta\omega = \pm 0.5J$)

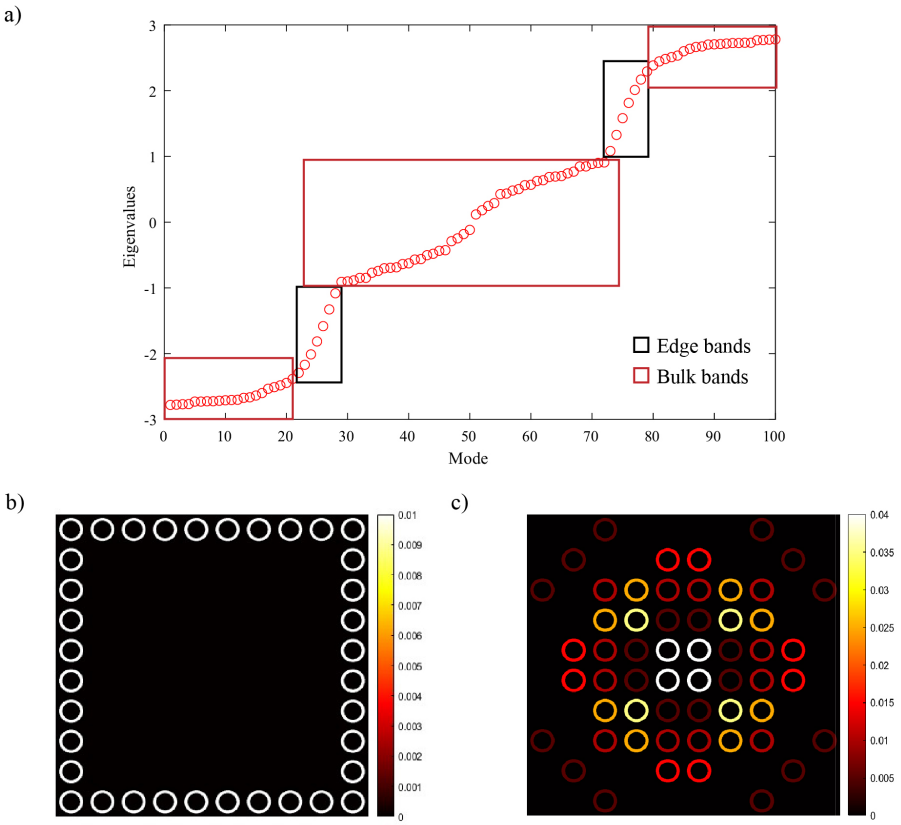


Figure 3.9: Eigenvalues and eigenfunctions for the topological 2D lattice simulating the integer quantum Hall model for photons, showing edge and bulk bands and their corresponding eigenfunctions.

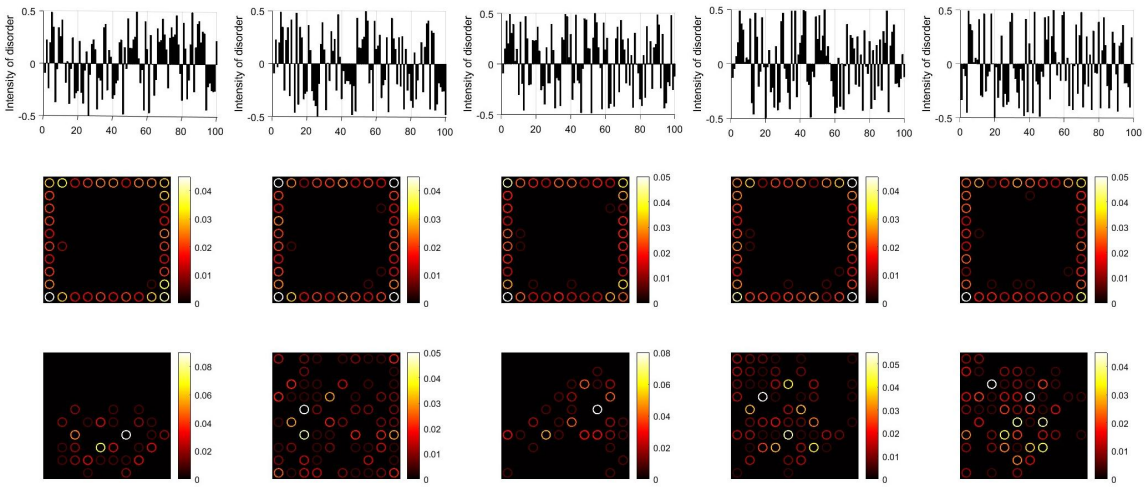


Figure 3.10: Robustness of edge states

on the ring resonance frequencies ω_0. We clearly see that the eigenfrequencies corresponding to the edge states are very robust against these intensive disorders whereas those of the bulk states are very susceptible to the disorder.

In experimental realizations, the synthetic magnetic flux is introduced using two sets of ring resonators, called the site and the link rings [21, 22]. The link rings are positioned asymmetrically between the site rings which leads to the introduction of a direction-dependent hopping phase between the site rings. Furthermore, in an experimental realization, the disorder originates from the inherent imperfections in the fabrication process that lead to random variations in the ring resonance frequencies, their coupling strengths, and also the hopping phases ϕ_n.

Chapter 4

Engineering Supermodes using Fourier techniques

As we discussed in the last chapter, near a single resonance frequency of the rings, coupled resonator arrays can be conveniently described using the tight-binding Hamiltonian formalism. The eigenvalues and the corresponding eigenfunctions of this Hamiltonian yield the resonance frequencies and corresponding wavefunctions of the supermodes of the resonator arrays. We note that we mostly considered uniform arrays with identical ring resonance frequencies and uniform coupling strengths.

In this chapter, we will explore the possibility of engineering the eigenvalues and eigenfunctions of supermodes using Fourier transform techniques, for example, by detuning the ring resonance frequencies in a sinusoidal pattern. Using these techniques, the goal is to selectively target the resonance frequencies of a given set of supermodes. We find that depending on the boundary conditions (OBC, PBC) of the coupled resonator array, a different scheme is required to engineer the eigenfrequencies of the supermodes. More specifically, for 1D resonator chains with open-boundary conditions, we can target a given supermode by varying the ring resonance frequencies. In contrast, for a 1D resonator chain with periodic boundary conditions (PBC), we need a controlled coupling (back-scattering) between CW and CCW propagating modes of a single-ring resonator.

These techniques are motivated by the recent demonstrations of engineering the longitudinal modes of single-ring resonators [28, 29, 30]. For example, a sinusoidal variation along the ring waveguide width, and therefore, the effective refractive index, manifests as a coherent back-scattering that couples forward and backward propagating waves for only one of the longitudinal modes and lifts their degeneracy.

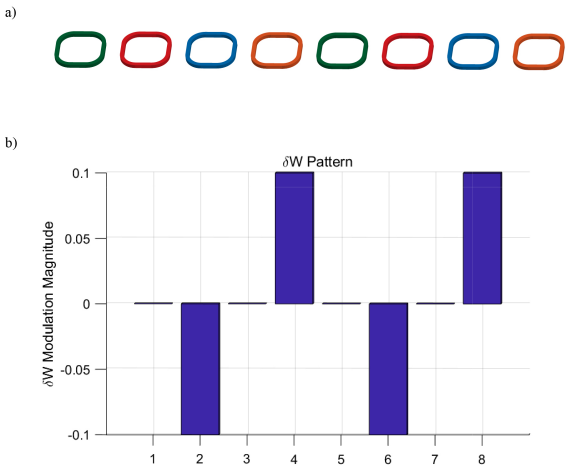


Figure 4.1: a. Schematic of a 1D resonator chain with OBC and modulated ring resonance frequencies. An example modulation pattern is shown in b.

4.1 Engineering 1D Chains with OBC

As our first example of engineering supermodes of coupled resonator arrays, we investigate a 1D resonator chain with open boundaries. For a uniform array, with identical ring resonance frequencies and uniform coupling strengths, the Hamiltonian and the calculated eigenvalues and eigenfunctions were discussed in Section 3.3. Here, we introduce a sinusoidal modulation (time-independent) on ring resonance frequencies as a function of the position of the ring along the chain (see Figure 4.1). This modulation is written as

$$\delta\omega\left(n\right) = \delta\omega_0 \; sin\left(2\pi f \; \frac{n}{N}\right), \tag{4.1}$$

where $\delta\omega_0$ is the strength of modulation, f is the frequency factor of modulation, n is the index corresponding to the position of the ring in the chain.

With this modulation, the Hamiltonian takes the form

$$H = \sum_{n=1}^{N} \left(\omega_0 + \delta\omega\left(n\right)\right) a_n^\dagger a_n - J \sum_{n=1}^{N-1} a_{n+1}^\dagger a_n - J \sum_{n=1}^{N-1} a_n^\dagger a_{n+1}. \tag{4.2}$$

Figure 4.2 shows the calculated eigenvalues of this modulated Hamiltonian for an $N = 40$ resonator chain with $f = 10,\ \delta\omega_0 = 0.2\ J$ and compares it with those of the original Hamiltonian ($\delta\omega_0 = 0$). We find that modes 10, 11 show a significant shift in their resonance frequency. The resonance frequency of mode 10 is shifted down whereas that of mode 11 is shifted up. In Figure 4.2,

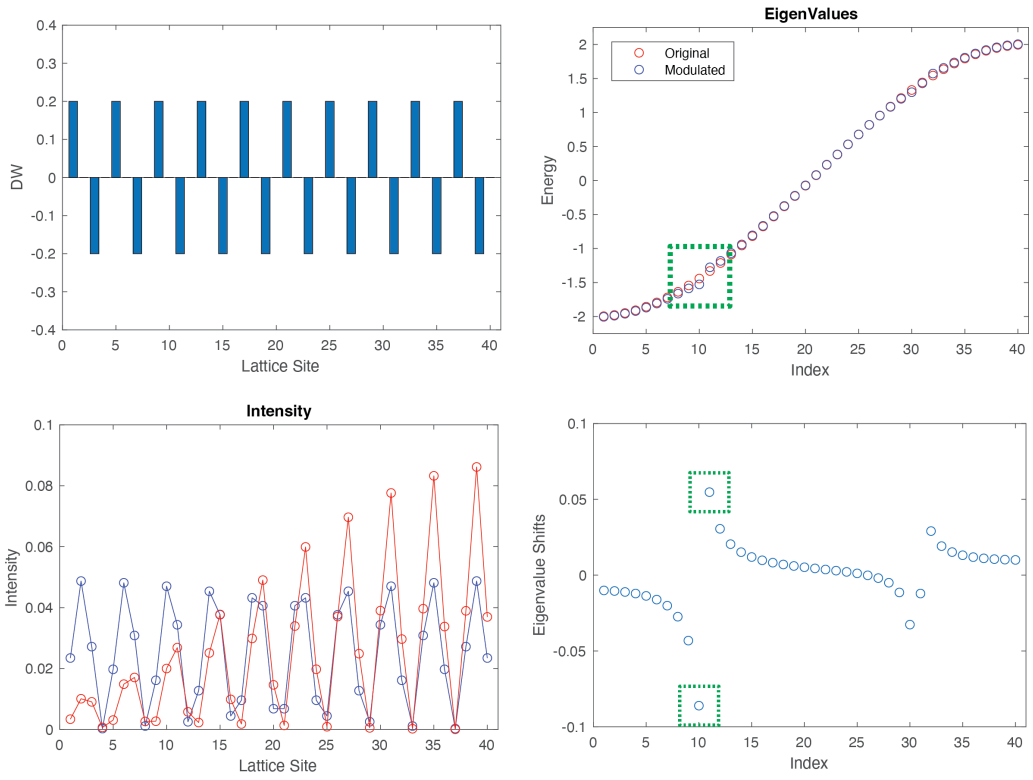


Figure 4.2: 1D chain of 40 resonators with OBC: modulation pattern, a comparison of original and modulated eigenvalues, and the intensity pattern before and after modulation.

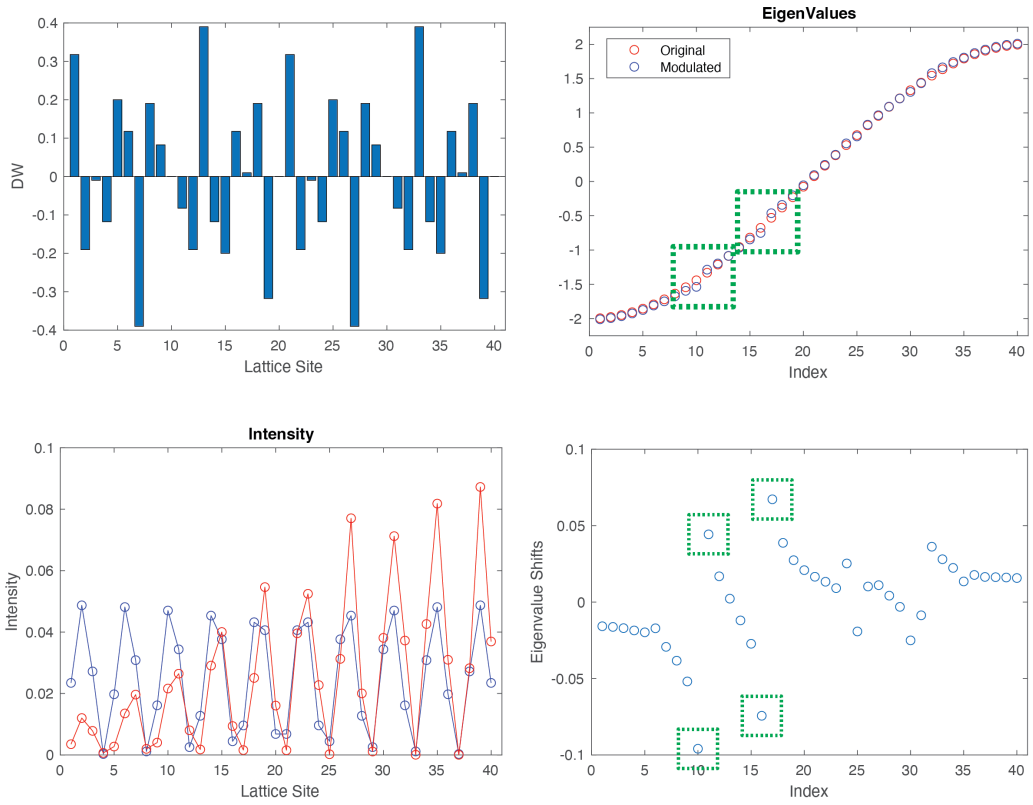


Figure 4.3: 1D chain of 40 resonators with OBC: modulation pattern as a sum of two frequencies, a comparison of original and modulated eigenvalues, and the intensity pattern before and after modulation.

we also compare the corresponding intensity profiles in the array for the original and the modulated Hamiltonian and find that both exhibit a standing-wave pattern as expected.

To understand this relatively selective shift of a single eigenmode using a sinusoidal modulation, we note that the modes of the 1D resonator chain with OBC are standing waves with different spatial frequencies, and are therefore, orthogonal. Therefore, a sinusoidal modulation with a given spatial frequency predominantly affects the mode that has the same spatial frequency (see Figure 4.2).

We can extend this modulation scheme such that we use a sum of two different sinusoidal modulation patterns with different frequencies, that is,

$$\delta\omega\left(n\right) = \delta\omega_1 \, sin\left(2\pi f_1 \, \frac{n}{N}\right) + \delta\omega_2 \, sin\left(2\pi f_2 \, \frac{n}{N}\right), \tag{4.3}$$

In Figure 4.3, we show the corresponding results for $N = 40$, $f_1 = 10$, $f_2 = 16$, $\delta\omega_1 = \delta\omega_2 = 0.2\ J$. Now, we find that the set of eigenmodes 10,11 and 16,17 are shifted the most.

The energies of modes 10 and 16 are shifted down, whereas those of modes 11 and 17 are shifted up. As before, we find that the eigenmode energies are shifted in pairs, one mode shifting down and a neighboring mode shifting up. The intensity profiles in the lattice still retain their standing-wave behaviour.

In Figure 4.2 and Figure 4.3, we also observe significant shifts in resonance frequencies of neighboring modes. These unintended shifts are because of the discrete nature of the modulation pattern. In Chapter 5, we will attempt to use genetic optimization techniques, in addition to the Fourier techniques, to minimize these unintended shifts.

4.2 Engineering 1D Super-rings with PBC

In this section, we focus on engineering eigenvalues of 1D coupled resonator chains with periodic boundary conditions. As we discussed in the last chapter, the modes of 1D chains with PBC are traveling waves that circulate around the lattice in clockwise and counter-clockwise directions. Furthermore, these modes exhibit a two-fold degeneracy.

As before, we use a sinusoidal modulation pattern of the ring resonance frequencies. For this demonstration, we chose $N = 40$ and a modulation pattern

$$\delta\omega\left(n\right) = 0.2\ sin\left(2\pi 10\ \frac{n}{N}\right), \tag{4.4}$$

such that the amplitude of modulation $\delta\omega_0 = 0.2$ and frequency factor $f = 10$. Figure 4.4 shows the modulation pattern and a comparison of the original eigenvalues and the modulated eigenvalues. In this case, we find that two sets of modes $n = 10, 11$ and $n = 30, 31$ show significant shifts in eigenvalues. The energies of modes 10 and 30 are shifted down, and those of modes 11 and 31 are shifted up. The first set of modes that show shifts coincides with the frequency of modulation f and the second coincides with $N - f$. Furthermore, this is in stark contrast to the 1D chain with OBC where only one set of modes shows significant shift.

On closer inspection, we also find that this modulation pattern on the ring resonance frequencies breaks the two-fold degeneracy of only these two pairs of modes (10-11 and 30-31). In each pair, one of the modes is shifted towards higher energy and the other towards lower energy. The other modes, although shifted in frequency, retain their degeneracy.

In Figure 4.4 we also plot the intensity distributions for the 10^{th} mode before and after modulation. Before modulation, the mode exhibits a uniform intensity distribution which is consistent with that of a traveling-wave resonator. However, after the modulation, the split modes exhibit a

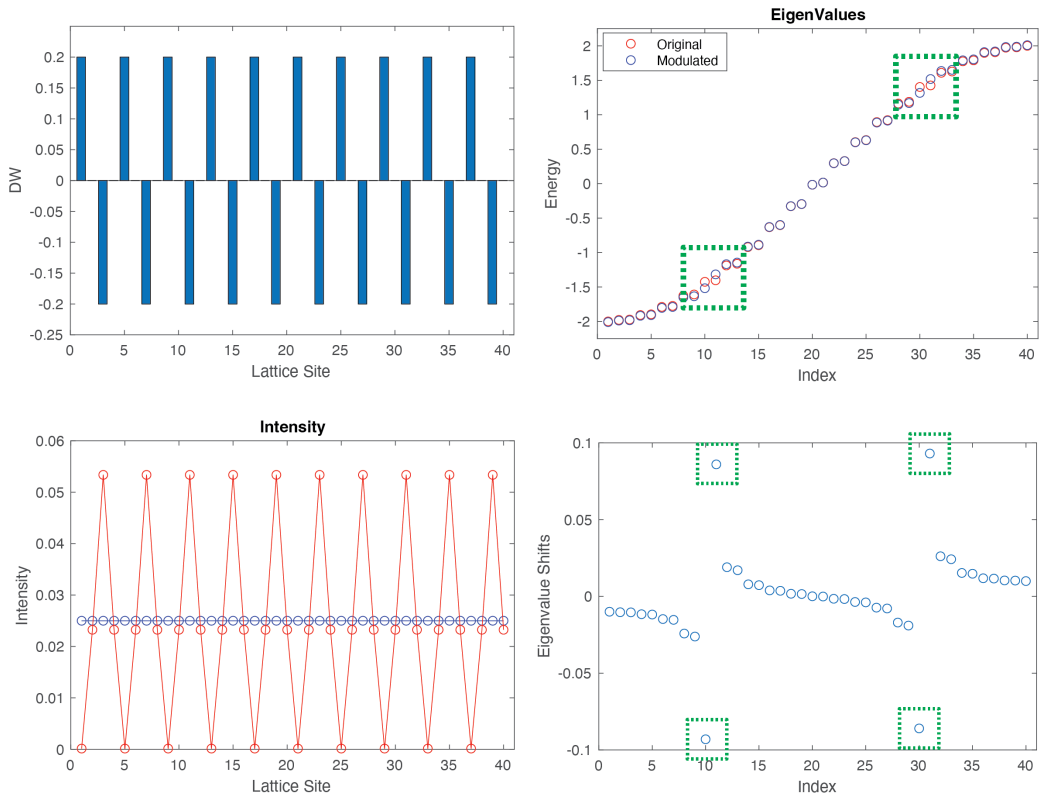


Figure 4.4: 1D chain of 40 resonators with PBC: modulation pattern as a single frequency, a comparison of original and modulated eigenvalues, and the intensity pattern before and after modulation.

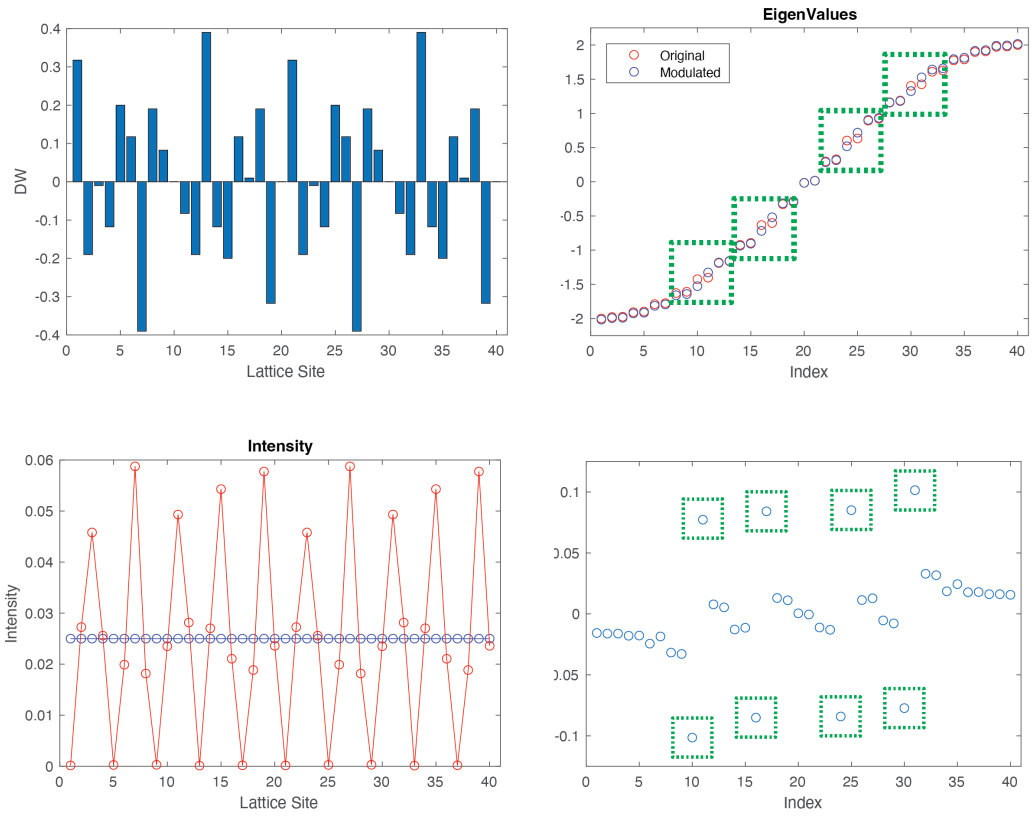


Figure 4.5: 1D chain of 40 resonators with PBC: modulation pattern as a sum of two frequencies, a comparison of original and modulated eigenvalues, and the intensity pattern before and after modulation.

standing-wave type intensity pattern that indicates modulation-induced coupling of forward and backward propagating modes. This coupling is consistent with the splitting of the eigenvalues observed in Figure 4.4. These results are interesting in the sense that all the modes of the super-ring are of the traveling-wave type with equal intensity distribution at each resonator. Even then, a sinusoidal modulation breaks the degeneracy of only two pairs of modes.

As before, we can extend this scheme to introduce a sum of two modulation patterns with different frequencies of the form

$$\delta\omega\,(n) = \delta\omega_1\; sin\left(2\pi f_1\;\frac{n}{N}\right) + \delta\omega_2\; sin\left(2\pi f_2\;\frac{n}{N}\right), \tag{4.5}$$

where $f_1,\ f_2$ are the two modulation frequencies, and $\delta\omega_1,\ \delta\omega_2$ are their respective amplitudes. In Figure 4.5, we plot the original and modulated eigenvalues for $N = 40$, $f_1 = 10$, $f_2 = 16$, and $\delta\omega_1 = \delta\omega_2 = 0.2\ J$. As expected, we now observe a splitting of four sets of modes at

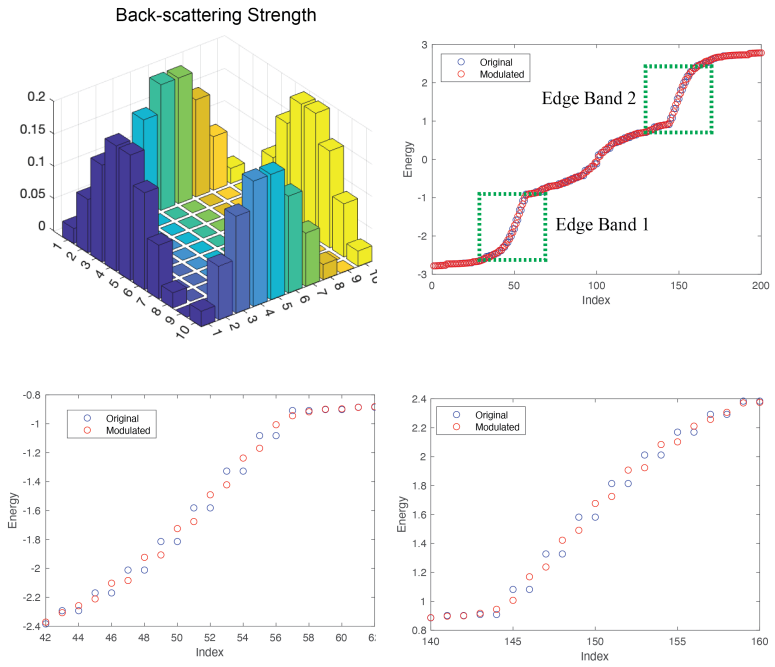


Figure 4.6: Engineering edge modes of the topological 2D resonator array using back-scattering.

$n = (10, 11)$, $(30, 31)$, $(16, 17)$, $(24, 25)$ in Figure 4.5. These results indicate that we could create more complex modulation patterns for ring resonance frequencies to introduce greater control over the eigenmode structure.

4.3 Engineering Back-scattering in 2D Lattice with Synthetic Magnetic Field

In this section, we will discuss the engineering of the supermodes, in particular the edge modes, of the topological 2D array with a uniform synthetic magnetic field. The goal will be to shift the eigenenergy (resonance frequency) of only one or a pair of edge states. The edge modes circulate around the lattice boundary and are, in some sense, similar to the supermodes of the super-ring (1D array with periodic boundary conditions). Similar to the super-ring, they exhibit CW and CCW circulating edge states around the lattice that form a traveling-wave super-resonator. However, unlike the 1D super-ring, the CW and CCW circulating edge states are not degenerate in frequency and are separated by a large gap in the order of the coupling strength J. This broken degeneracy is a result of the synthetic magnetic field.

This lack of degeneracy between CW and CCW edge states also leads to another major distinction between the edge modes and the modes of the 1D array - the edge modes are robust against variations in ring resonance frequencies. We showed this robustness of edge states against random variations of ring resonance frequencies in Figure 3.10. Therefore, we can easily conclude that creating a sinusoidal modulation pattern of ring resonances, as we did for the 1D chain, will not work.

Therefore, we can resort to another degree of freedom, that is, the pseudospin of the single-ring resonators - that is the circulation direction of light within each ring. The two pseudospins (CW and CCW) form time-reversed partners. If at a given frequency, the edge states corresponding to one pseudospin (say CW in individual rings) circulate around the lattice in a CW direction, then at the same frequency, the edge states corresponding to the other pseudospin (CCW) will circulate around the lattice in CCW direction. In other words, at a given frequency, the edge states corresponding to the two pseudospins circulate in opposite directions around the lattice.

In the absence of any back-scattering in the rings, these pseudospins are decoupled, that is, they are degenerate in frequency and each of them constitutes a traveling-wave super-resonator. However, by introducing a back-scattering in each ring, we can couple the two pseudo-spins (at the same frequency), and therefore, the CW and CCW propagating edge states. This coupling of CW and CCW modes can then create a standing-wave pattern in the lattice.

Following our description of Chapter 2, of the pseudospin and the back-scattering induced coupling, we simulated the introduction of back-scattering on the ring resonators located at the edge of the lattice. As before, we introduce a sinusoidal modulation of the back-scattering strength along the edge, and the results are shown in Figure 4.6. We find that this coupling indeed breaks the degeneracy between the two pseudospins and creates a standing-wave like intensity pattern along the edge of the lattice. However, the modulation pattern simultaneously splits the degeneracy of all the edge modes, in both the edge bands. We tried modulation patterns with different frequencies, but we were not able to shift the resonance frequency of a selected edge state resonance. This is probably because of the unique topological characteristics and the robustness of edge states.

Chapter 5

Engineering Supermodes using Genetic Optimization

As the results in Chapter 4 show, by applying a sinusoidal modulation pattern on the individual resonator frequencies, we can engineer the resonance frequencies of the supermodes of the 1D coupled resonator arrays. The goal was to shift the resonance frequencies of a target supermode or a set of supermodes. Nevertheless, we found that the supermodes other than the target super modes are also shifted in their resonance frequencies to a significant extent. In this chapter, we show that by using a genetic-optimization (GO) based inverse-design approach, we can significantly improve the selective engineering of target supermodes. This approach also overcomes some of the limitations of simple sinusoidal modulation patterns. For example, using sinusoidal modulation of a single frequency, we always found a pair of neighboring modes were shifting up/down in energy. By using GO, we can shift only one supermode without significantly impacting other supermodes.

5.1 Genetic Optimization Algorithm

Genes play a pivotal role in genetics and are the most basic unit of inheritance. By coding the construction of protein structures, genes influence numerous characteristics of the body and behavior. The DNA sequences of a species contain a large number of genes that are randomly mutated by the environment, shuffled and recombined during sexual reproduction, providing a huge diversity of options for the species. Individuals with advantageous traits are more likely to survive and reproduce under the selection of natural conditions. Such processes drive evolution and allow species to become more adapted to their environments.

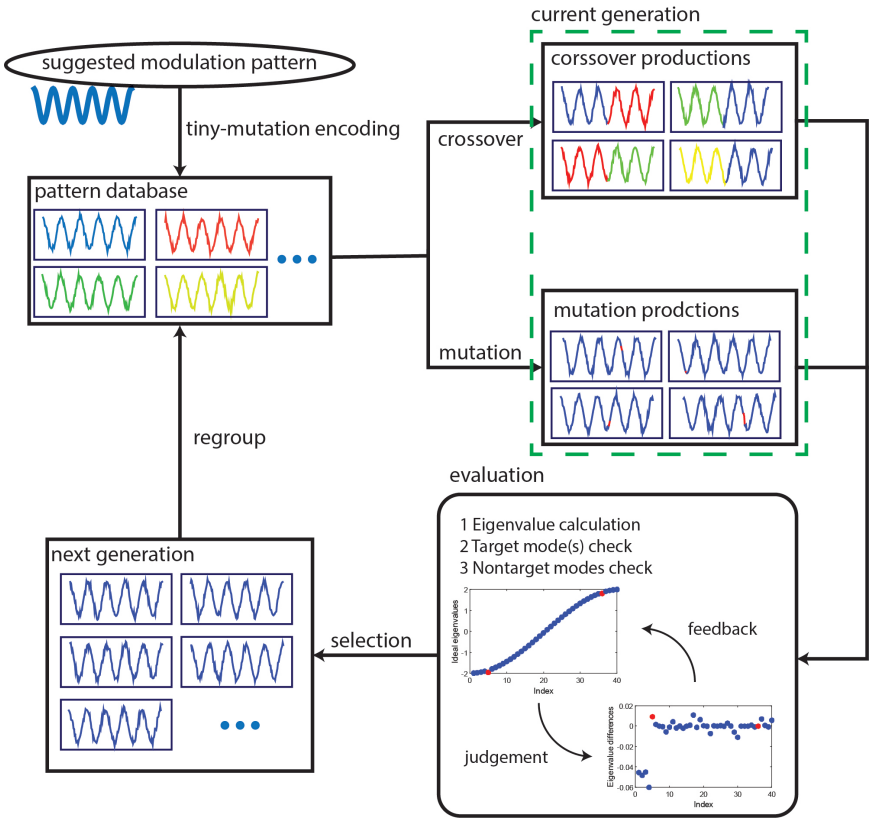


Figure 5.1: The specific Genetic Algorithm process in Ring Resonator Array Optimization.

The concept of genetic algorithms(GA), which are solutions that mimic the process of natural selection described above, was introduced by John H. Holland [32]. Holland's main realization was that the mechanisms of natural selection and genetics could be abstracted and applied to engineering problems. First, potential solution patterns were encoded into DNA-like data strings. Then, mutation and crossover operations are performed to produce new generations of data. The new generations are evaluated and selected for survival based on engineering requirements. By continually repeating the above process, the solution population evolves towards better outcomes. In recent years, there have been very many successful demonstrations of this optimization approach for photonic applications [33, 34, 35].

Here, we apply the genetic optimization algorithm to engineer supermodes of couple resonator arrays. A pictorial description of the optimization process is shown in Figure 5.1. We start with a sinusoidal modulation pattern that will approximately shift the resonance frequencies of target supermodes, and also impose unintended shifts on supermodes. Small-mutation perturbations on

the suggested sinusoidal modulation patterns create many derivative patterns and generate the initial database. Subsequently, we implement mutation and recombination processes and evaluate population of the mutated generation. The evaluation quantifies the difference between the eigenvalues of the current generation and the desired supermode eigenvalues (with desired shifts) and then selects optimal (fit) solutions to form a new database. This cycle completes one iteration of the algorithm. We continue iterating until the algorithm converges to the optimal solution within specified tolerances. We implement this optimization using the inbuilt 'ga' algorithm in Matlab.

In the following, we will show some examples of the genetic optimization of supermodes of 1D resonator arrays, and compare them against those obtained using simple Fourier-transform-based sinusoidal modulation schemes presented.

5.2 Engineering supermodes in 1D resonator arrays with OBC

In this section, we present our results for the optimization of 1D resonator arrays with open-boundary conditions. As a first step towards this goal, we quantify the fitness of a given member of a population, that corresponds to a set of individual ring resonance frequencies, using a parameter Γ defined as

$$\Gamma = \sum_{i=1}^{N} \left(\gamma(i)\,|E(i) - E_0(i)|\right)^2 \tag{5.1}$$

where E is the set of calculated supermode eigenvalues for a given member of the population corresponding to a set of individual ring resonance frequencies. E_0 is the set of target supermode eigenvalues. We use $\gamma(i)$ as a weighting array that can screen for the fitness of a given eigenmode (a given trait in the population).

Using this GA screening criterion, we implemented the optimization algorithm in Matlab for a chain with $N = 40$ resonators and OBC. One example result is shown in Figure 5.2. Here we target the shift of a single supermodes with indexes 8 and 9. As we saw in Chapter 4, the application of a sinusoidal modulation of the ring resonance frequencies, with spatial frequency $f = 8$, shifts a pair of modes with index 8 and 9 such that the energy of the 8^{th} mode is shifted down and the 9^{th} mode is shifted up. In addition, eigenvalues of other supermodes are also shifted to a large extent. In particular, modes $32 = 40 - 8$ and 33 show a significant shift, almost as large as modes 8 and 9.

After genetic optimization, we find that the errors, that is, the unintended shifts in other supermodes (other than 8^{th} and 9^{th}) are significantly reduced. The maximum unintended shift error,

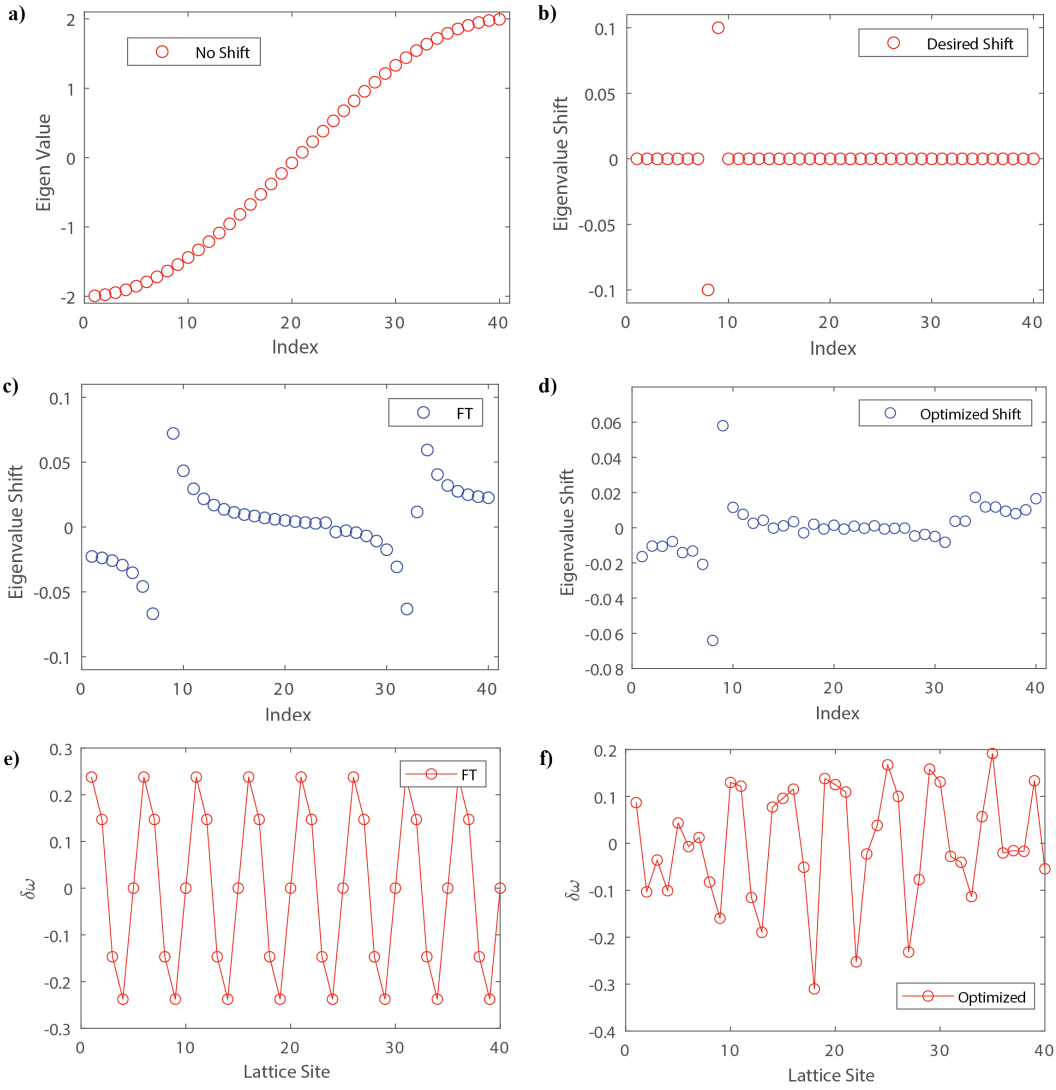


Figure 5.2: Optimization of a 40-ring 1D array with OBC where one pair of modes are shifted. We choose $\delta W = 0.2$, $f = 8$, and $\gamma_i = 1.0$ for all modes. a) The eigenvalues before any modulation. b) The desired shifts δE in supermode eigenvalues, c)the shifts achieved after FT, and d) the shifts after GO. e) The shifts in ring resonance frequencies from the sinusoidal modulation and f) after GO.

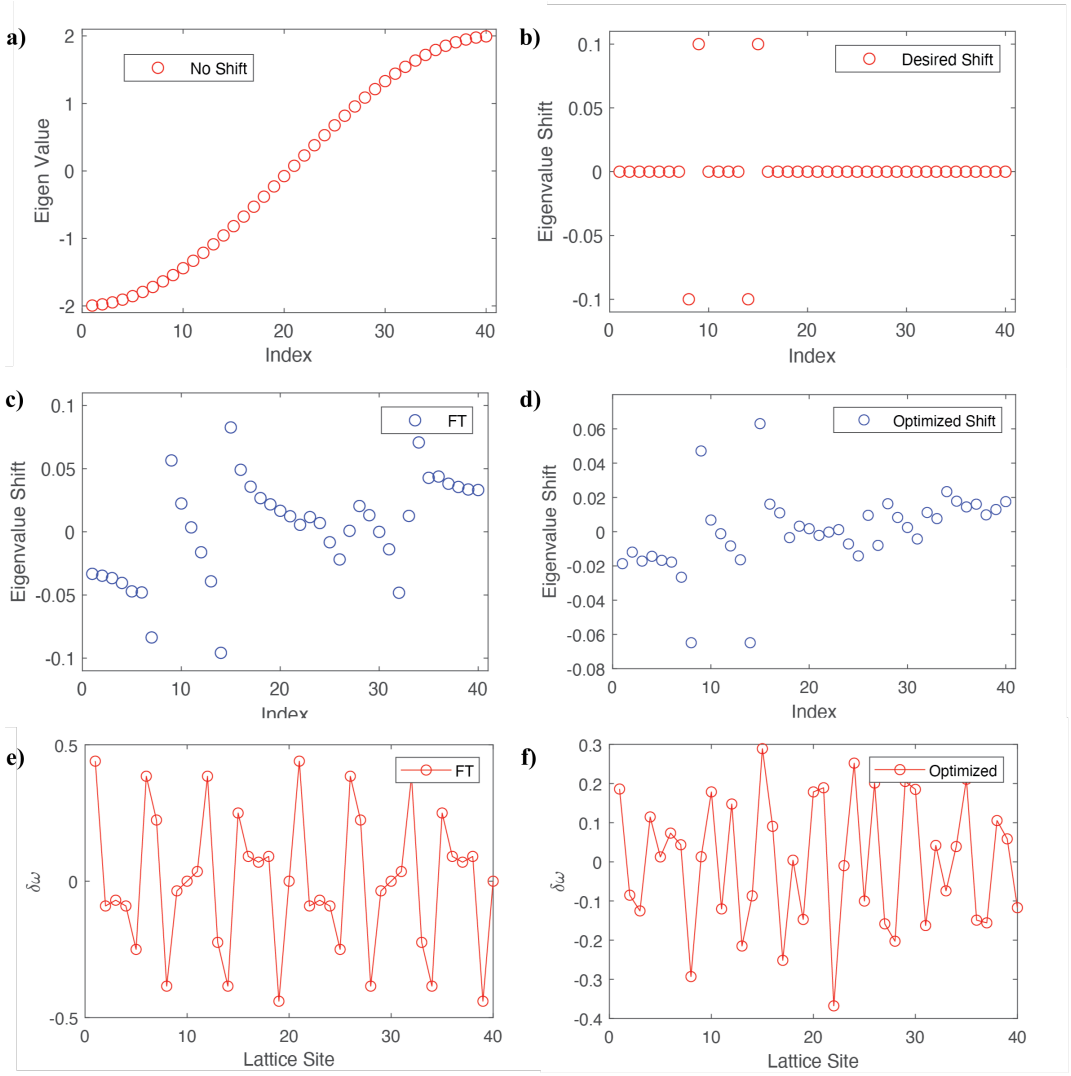


Figure 5.3: Optimization of a 40-ring 1D array with OBC where two pairs of modes are shifted. We choose $\delta W_1 = \delta W_2 = 0.2$, $f_1 = 8$, $f_2 = 14$ and $\gamma_i = 1.0$ for all modes. a) The eigenvalues before any modulation. b) The desired shifts δE in supermode eigenvalues, c)the shifts achieved after FT, and d) the shifts after GO. e) The shifts in ring resonance frequencies from the sinusoidal modulation and f) after GO.

which was in modes 32 and 33, is now reduced from about 0.06 to about 0.02. We also note that the shifts ($\delta\omega$) in resonance frequencies of individual resonators after GO show a modulation pattern that is very similar to the sinusoidal modulation with frequency $f = 8$. These results clearly indicate that the GO algorithm is performing better than the simple sinusoidal modulation pattern for the 1D chain with OBC.

We extended this technique to include shifts in two sets of modes $(8, 9)$ and $(14, 15)$. This is the same shift that we attempted using the sum of two sinusoidal modulations with frequencies $f_1 = 8,\ f_2 = 14$. In Figure 5.3, we show the results before and after GO. Once again, we find that with the sinusoidal modulation, there are significant errors, that is, unintended shifts in modes other than the target modes. However, after GO, these errors are significantly reduced.

Next, we attempted to optimize the 40 resonator chain where only one of the target modes (here 8^{th}) is shifted (Figure 5.4). As we saw, the sinusoidal modulation is not able to achieve such a shift because it always shifts resonances in pairs. Nevertheless, using GO, we did achieve the desired results, that is, only mode 8 was shifted down in energy whereas all other modes showed significantly reduced shifts of the order of $0.02\ J$. Even in this case, we find that the resonance frequency shifts on individual resonators show some oscillation pattern that is reminiscent of the original sinusoidal modulation.

We attempted to achieve more complex shifts, for example, where only two or three modes, but of different pairs were shifted (see Figure 5.5, and Figure 5.6). Both these engineered spectra can not be achieved using simple sinusoidal modulations. However, for both these cases, GO achieved supermode spectra that are very close to the desired spectra.

We note that the implementation and efficiency of this optimization algorithm in Matlab depends on several key factors including the population size P of each generation, constraint tolerance Δ, and elite count EC which is the fraction of the population in each generation that passes on to the next generation without any mutations. Larger population size and elite count raise the precision but also the processing time for optimization. For the results presented in Figure 5.2, we choose $P = N^3$ and $EC = 0.1 * P$, where N is the number of resonators in the array. Constraint tolerance Δ is chosen to be 10^{-6} such that the optimization process stops when the improvement in fitness Γ is less than this threshold. For all cases, we found that the error in the best candidate of each generation was optimized after as small as 30-50 generations, and iterating the algorithm beyond this number only reduced the mean error of the population. The best candidate error did not change much.

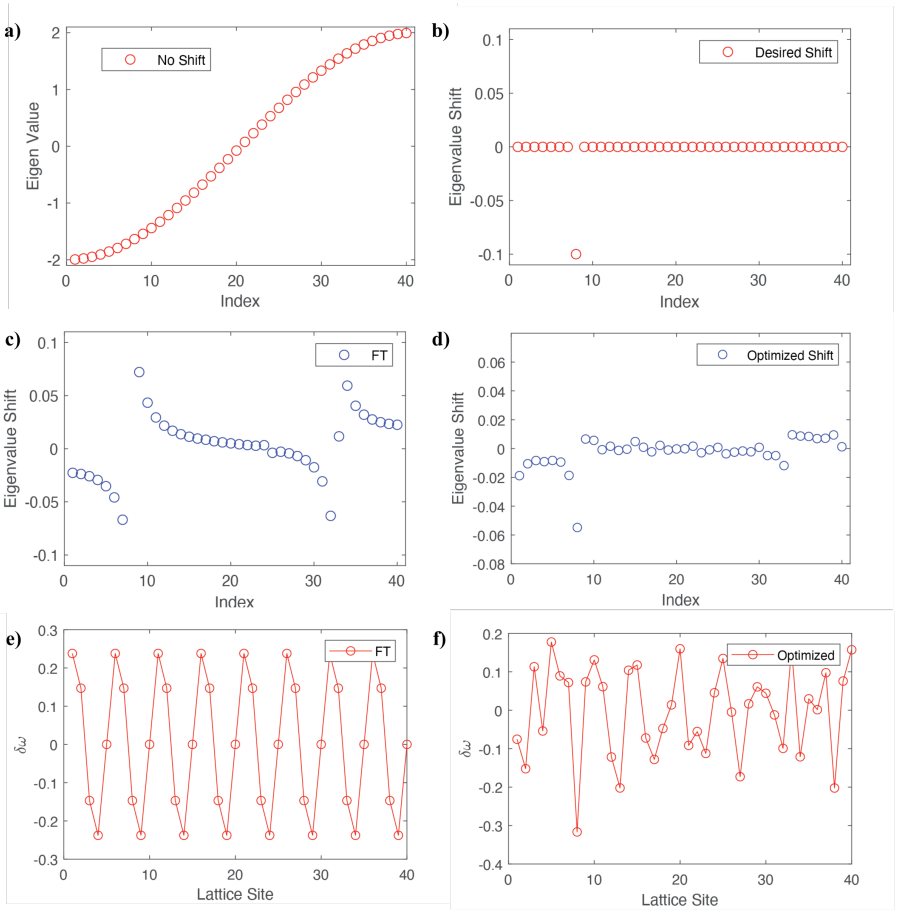


Figure 5.4: Optimization of a 40-ring 1D array with OBC where only one mode is shifted. We choose $\delta W_1 = 0.2$, $f = 8$, and $\gamma_i = 1.0$ for all modes. a) The eigenvalues before any modulation. b) The desired shifts δE in supermode eigenvalues, c)the shifts achieved after FT, and d) the shifts after GO. e) The shifts in ring resonance frequencies from the sinusoidal modulation and f) after GO.

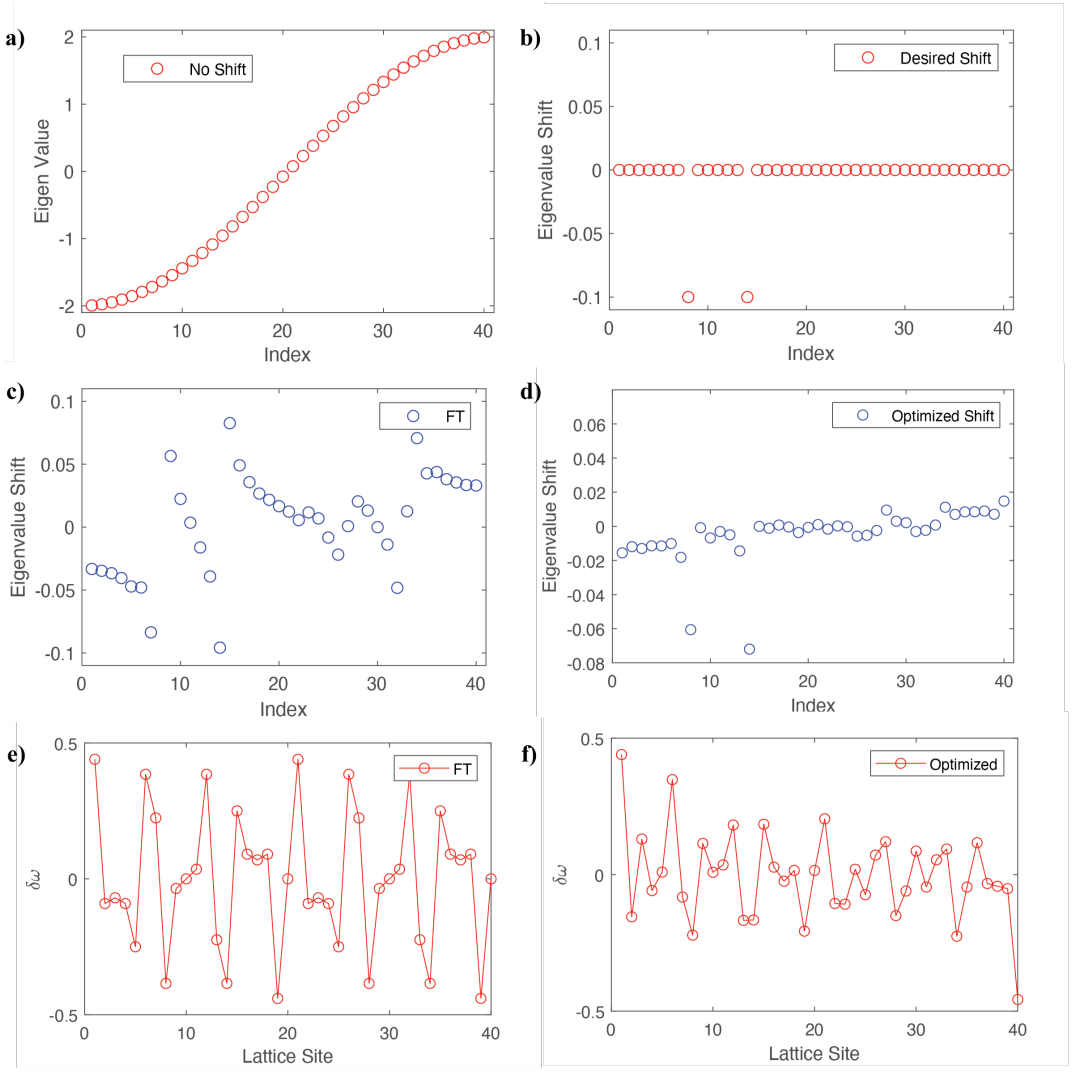


Figure 5.5: Optimization of a 40-ring 1D array with OBC where two modes, from different pairs, are shifted. We choose $\delta W_1 = \delta W_2 = 0.2$, $f_1 = 8$, $f_2 = 14$ and $\gamma_i = 1.0$ for all modes. b) The desired shifts δE in supermode eigenvalues, c)the shifts achieved after FT, and d) the shifts after GO. e) The shifts in ring resonance frequencies from the sinusoidal modulation and f) after GO.

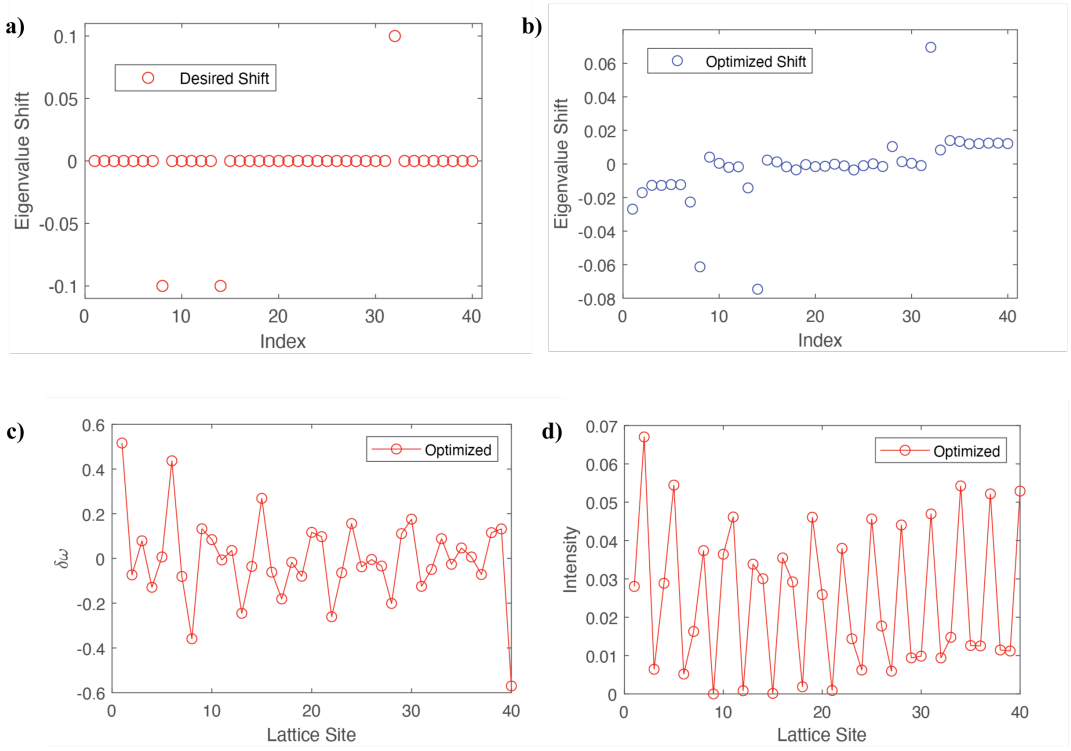


Figure 5.6: Optimization of a 40-ring 1D array with OBC, where three modes, all from different pairs are shifted. a) The desired shifts δE in supermode eigenvalues, b) the shifts achieved after GO. c) The shifts in ring resonance frequencies from the sinusoidal modulation and after GO. d) Intensities of the 14^{th} (one of the shifted modes) mode after GO.

5.3 Engineering supermodes in 1D resonator arrays with PBC

As we saw in Chapter 3, the supermodes of a super-ring - a 1D array with PBC are traveling waves with a two-fold degeneracy. In Chapter 4, we saw that a sinusoidal modulation of the ring resonance frequencies, with spatial frequency f, lifts the degeneracy of two pairs of supermodes $f, f+1$ and $N-f, N-f+1$.

In this section, we will address the question: can we use genetic optimization in 1D arrays to selectively shift the eigenvalues of only one pair of CW and CCW propagating supermodes? We emphasize that the traveling-wave nature of the supermodes dictates that selectively shifting only one supermode might not be feasible, and we have confirmed that this is indeed the case with GO.

Using a 40 resonator chain, with PBC, We first attempted to shift two pairs of modes $8, 9$ and $32, 33$ - exactly the same as those shifted by a sinusoidal modulation with frequency $f = 8$. The results are shown in Figure 5.6. As before, we see that the unintended shifts in other modes are reduced. However, compared to the OBC, the improvement in the errors is not that significant. That is simply because for the case of PBC, the sinusoidal modulation pattern works fairly well and the errors are small to begin with. We also note that the two-fold degeneracy of only the 8,9 and 32, 33 modes is broken, and that of all the other modes is well preserved in both cases.

Next, we attempted to optimize the array such that only one pair of modes, 8 and 9 are shifted. We found that the GO is not able to achieve this! Similar to the sinusoidal modulation, we always find two pairs of modes $(8, 9$ and $32, 33)$ that are shifted. This indicates that engineering supermodes of the 1D resonator super-ring with PBC are constrained by the symmetries of the array (such as the degeneracy of the CW and CCW propagating modes), and the GO is not able to break these underlying symmetries.

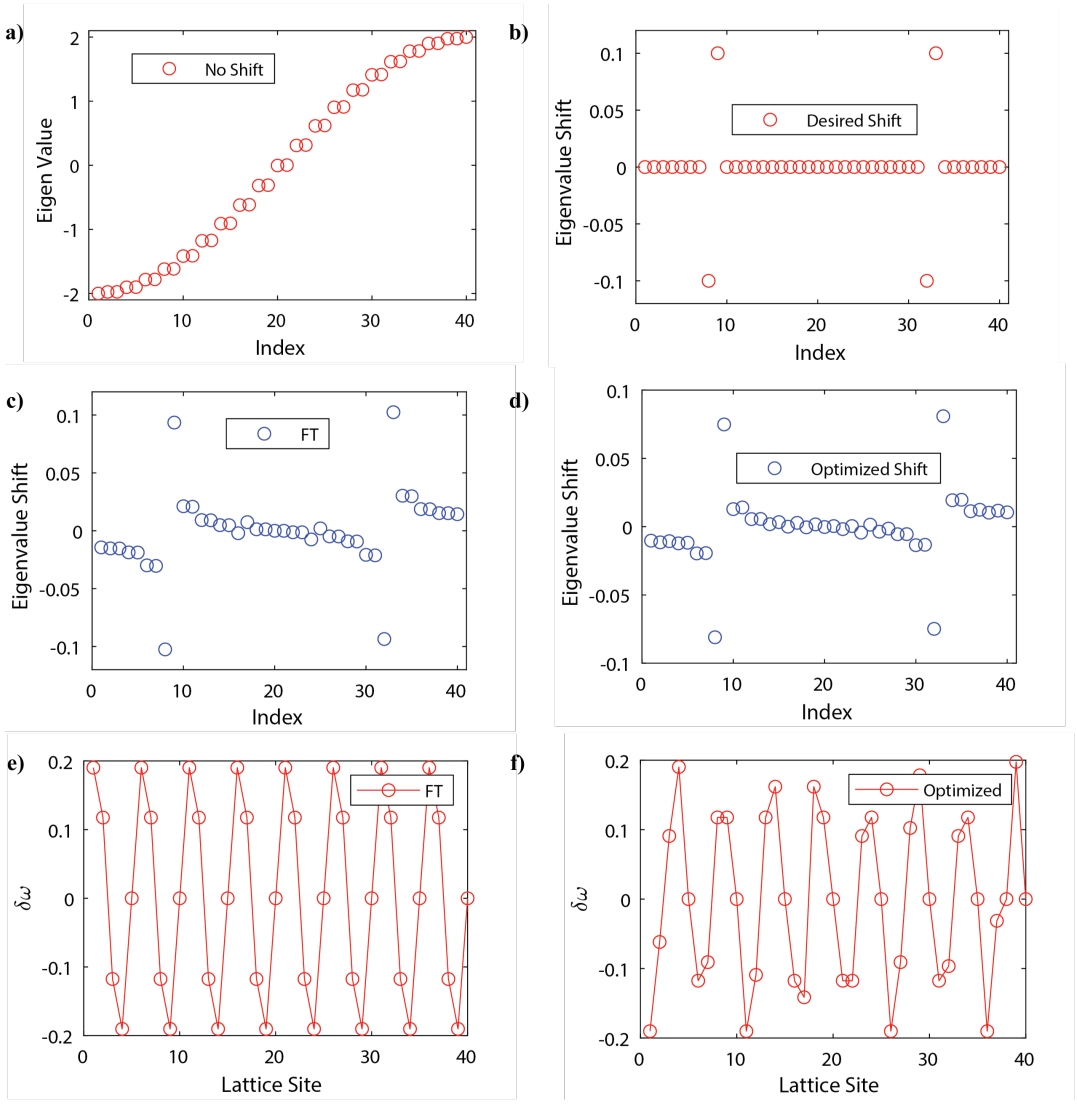


Figure 5.7: Optimization of a 40-ring 1D array with PBC, where two sets of modes, 8, 9, 32, and 33 are shifted. We choose $\delta W = 0.2$, $f = 8$, and $\gamma_i = 1.0$ for all modes. a) The eigenvalues before any modulation. b) The desired shifts δE in supermode eigenvalues, c)the shifts achieved after FT, and d) the shifts after GO. e) The shifts in ring resonance frequencies from the sinusoidal modulation and f) after GO.

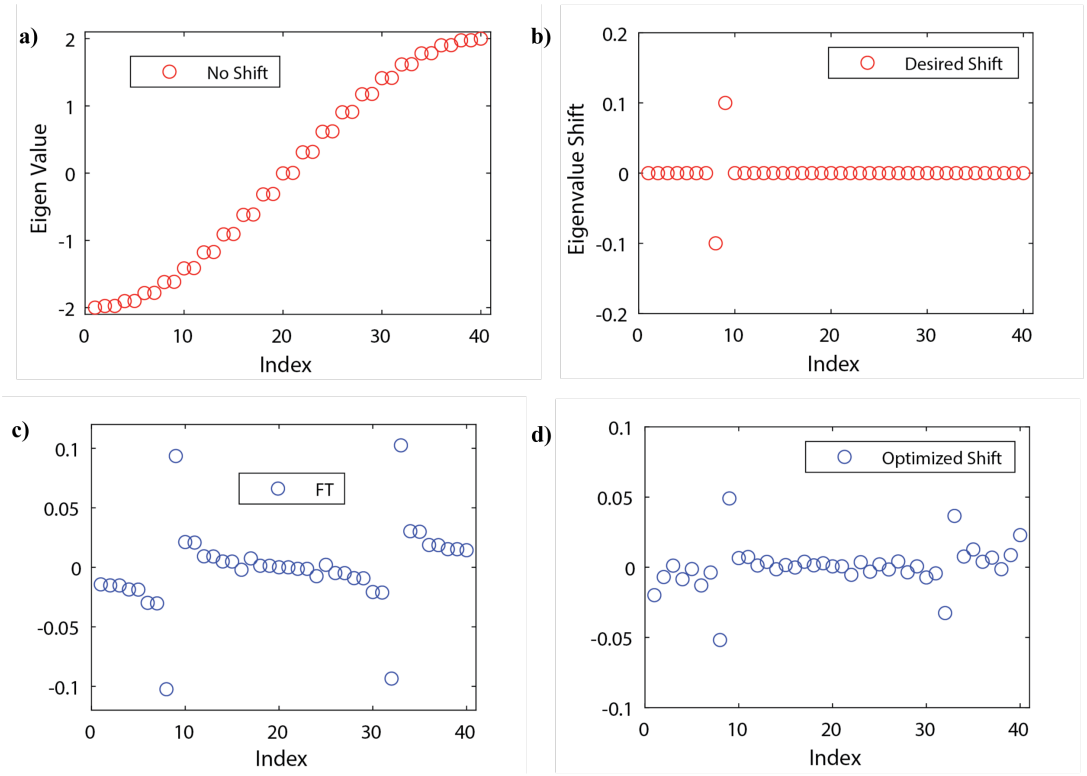


Figure 5.8: Optimization of a 40-ring 1D array with PBC, where only one set of modes, 8, 9, are shifted. We choose $\delta W = 0.2$, $f = 8$, and $\gamma_i = 1.0$ for all modes. a) Original eigenvalues, b) the desired shifts δE in supermode eigenvalues, c) the shifts achieved after FT, and d) the shifts after GO. GO is not able to achieve the desired eigenmode spectrum.

Chapter 6

Spectral Engineering of Coupled Resonator Quantum Light Sources

Sources of quantum light, such as single photons and entangled photon pairs, enable a number of quantum technologies such as secure quantum communications, quantum-enhanced sensing, and quantum computation [36]. Using quantum light, secure quantum communications between a ground station and a satellite have been demonstrated very recently. Similarly, quantum computation, in the form of Boson sampling, has also been demonstrated using quantum light sources.

Most of these demonstrations use quantum light generated using nonlinear spontaneous parametric processes such as the Spontaneous Parametric Down Conversion (SPDC) and spontaneous four-wave mixing (SFWM) [37]. Both these nonlinear processes generate pairs of photons that could be entangled in energy-time (their frequency spectrum), polarization, spatial mode structure, or a combination of these degrees of freedom. While it is relatively easy to implement such nonlinear processes using free-space bulk optics, they are challenging to scale to many hundreds of photons that would be required for practically relevant algorithms in quantum computation and simulation.

A scalable route to generate entangled photon pairs is by implementing SPDC or SFWM processes on an integrated photonic chip using ring resonators that could be only a few 10s of μm in size [9, 10, 11]. The use of ring resonators provides resonant enhancement that leads to higher generation rates. Simultaneously, the longitudinal modes of ring resonators provide a means to implement frequency-bin entanglement that can subsequently be used to generate higher-dimensional entanglement and cluster states.

Very recently, coupled resonator arrays have been explored to further engineer the spectrum of generated quantum light. In particular, in 1D arrays of resonators, with open-boundary conditions, the supermodes of the array have been shown to control the number of spectral modes involved in the generation of entangled photon pairs [19, 20]. Similarly, the 2D topological ring resonator arrays have demonstrated the generation of quantum light with an engineered spectrum and also shown their robustness against fabrication disorders [24, 25]. Nevertheless, the supermodes of 1D and 2D resonator arrays are usually regularly spaced in frequency. This structure gives rise to a quantum frequency comb.

In this chapter, using 1D resonator arrays with periodic boundary conditions, we will show that modulating the ring resonance frequencies using a sinusoidal pattern (or their combination) can be used to selectively disable the generation of modes at a given supermode. Such engineered quantum light sources could be dynamically tuned, for example, using thermal heaters, and could find many applications in generating novel frequency-bin entangled quantum light states.

6.1 Quantum light generation using a single-ring resonator

The most commonly used quantum light sources on a photonic chip use single-ring resonators made of silicon or silicon nitride [9, 10]. The Kerr nonlinearity of these materials gives access to the SFWM process. In this process, two photons from a laser beam, called the pump beam annihilate and generate two daughter photons, called the signal and the idler photons. The SFWM process does not transfer any energy or momentum to the material such that the total energy and momentum of the photons are conserved. Therefore, if the angular frequency of the pump photons is ω_p and that of signal and idler photons is ω_s, ω_i, respectively, then energy conservation dictates that $2\omega_p = \omega_s + \omega_i$. Similarly, the momentum conservation dictates that $2k_p = k_s + k_i$, where $k_p,\ k_s,\ k_i$ are the momenta of the pump, signal and idler photons, respectively. For a ring resonator, at its resonance frequency, the phase acquired by photons satisfies the relationship $k\ L = m\ 2\pi$, where m is an integer corresponding to the longitudinal mode number. Therefore, for the SFWM process in a ring resonator, the momentum conservation relation can also be written as $2\ m_p = m_s + m_i$. If the pump, signal, and idler beams are positioned close to the resonance frequencies of the ring resonator, then $\omega_{p,s,i} = m_{p,s,i}\frac{2\pi c}{n_{eff}L}$. Neglecting dispersion, we can conclude that the relationship $2\ m_p = m_s + m_i$ satisfies both energy band momentum conservation. This implies that if we pump the mode with index m_p, then signal and idler photons are generated in modes m_s and m_i that are located symmetrically around the pumped mode (see Figure 6.1).

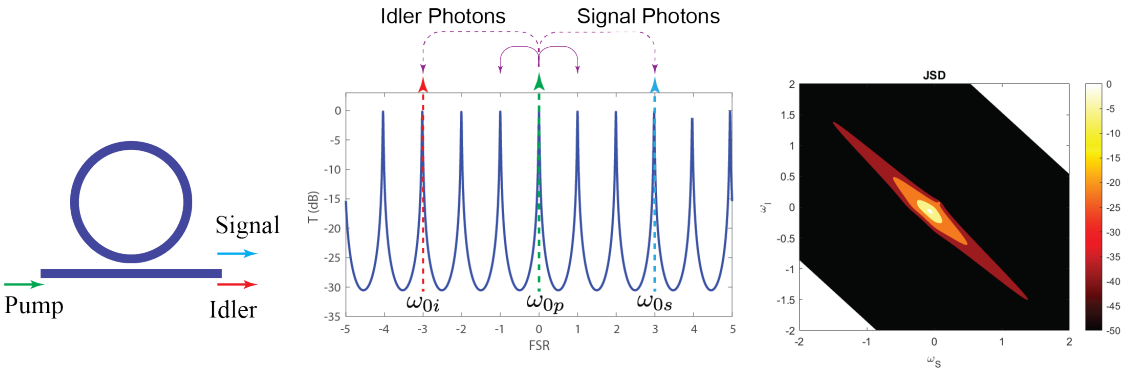


Figure 6.1: SFWM in a ring resonator. The signal and idler photon pairs are generated in modes located symmetrically around the pumped mode. Joint spectral intensity (JSI) calculated for a single-ring resonator showing energy-time entanglement between the generated signal and idler photons.

The signal and idler photons within a pair are spectrally correlated (entangled), but the photons from different pairs are independent and show no correlation. This spectral correlation structure gives rise to a quantum comb with roughly equally spaced spectral modes that coincide with the ring resonance frequencies.

The spectral correlations between each mode are depicted by the two-photon spectral wavefunction $\phi(\omega_s, \omega_i)$, such $|\phi(\omega_s, \omega_i)|^2$, referred to as the joint-spectral intensity(JSI) is the probability of simultaneously finding a signal photon at frequency ω_s and ω_i, and $\phi(\omega_s, \omega_i)|^2$, for a given input pump frequency ω_p. The numerically calculated JSI for a single-ring resonator is shown in Figure 6.1, for a pump frequency positioned at a resonance, that is, $\omega_p = \omega_{op}$, where ω_{op} is the resonance frequency corresponding to the pumped FSR. We specifically chose a pump with a narrow bandwidth. This choice naturally gives rise to the emergence of energy-time entanglement in the signal and idler photons. This entanglement is evident in the observation that the frequency of a generated idler photon ω_i is dictated by the frequency of corresponding signal photon ω_s. In other words, the two-photon spectral wavefunction is not factorizable $\phi(\omega_s, \omega_i) \neq f(\omega_s)\, g(\omega_i)$ - it can not be written as a product of independent spectral wavefunctions of the signal and idler photons.

6.2 Quantum light generation using a 1D resonator chain

As we discussed in Chapter 3, for a 1D resonator chain, each longitudinal mode resonance of a single ring splits into a number of supermodes that are the longitudinal modes of the array. In Figure 6.2 .a, we plot the eigenvalues for a 20 resonator chain with periodic boundary conditions

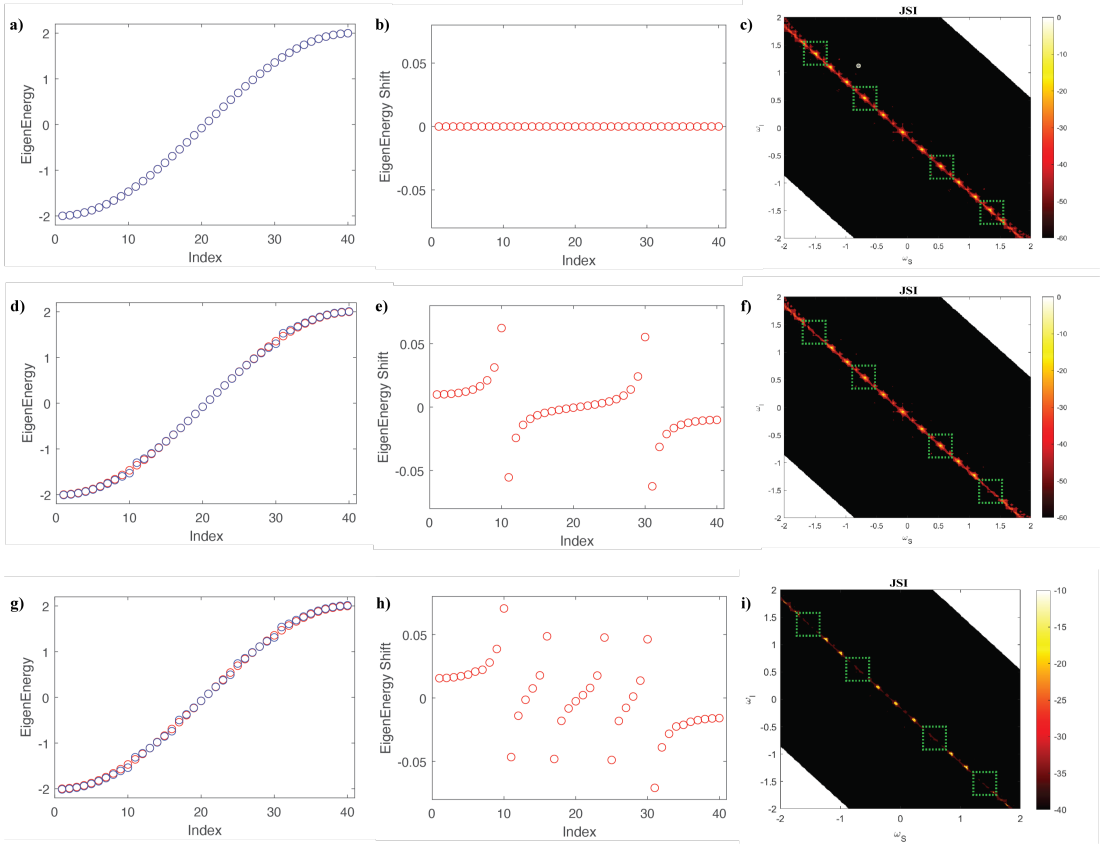


Figure 6.2: JSD for a 1D resonator chain with PBC, with and without modulations.

and a total synthetic gauge flux π. This flux breaks the degeneracy of the CW and CCW circulating modes around the lattice.

In Figure 6.2 .c, we plot the simulated JSI for this array with the pump frequency $\omega_p - \omega_{op} = 0.16J$, centered at one of the eigenvalues ($no.20$). We observe the formation of a quantum comb in the supermodes of the array such that there is a peak - the high intensity of generating signal and idler photons - at each pair of supermodes located symmetrically around the pumped mode. Similar to a single-ring resonator, the observed JSI in this case is not factorizable, and therefore, the generated signal and idler photons will be energy-time entangled.

To engineer this JSI for the resonator array, we introduce a sinusoidal modulation of the ring resonance frequency. As we saw earlier, this modulation targets a pair of modes that are located symmetrically around the resonance frequency ω_0 of the single-ring resonators.

As before, we introduce a sinusoidal modulation pattern on the ring resonance frequencies that affects the eigenvalues of only one pair of modes that are located symmetrically around ω_0. Here, we specifically use $\delta\omega\,(n) = \delta\omega_0\ sin\left(2\pi 12\ \frac{n}{N}\right)$. The resultant eigenvalue spectrum is shown in Figure 6.2 .d. The simulated JSI for this 1D chain with periodic modulation is shown in Figure 6.2 .f. We observe that a set of peaks, located symmetrically around the pump frequency, are missing from the JSI. This means that the generation of signal and idler photons at these shifted eigenvalues is no longer efficient. This is because of the shift in energy introduced by the modulation pattern that subsequently breaks energy conservation for these eigenmodes. This result clearly demonstrates the possibility of engineering spectral correlations generated using coupled multi-resonator arrays.

We can introduce a more complex modulation pattern that consists of a sum of two spatial frequencies, of the form

$$\delta\omega\,(n) = \delta\omega_1\ sin\left(2\pi f_1\ \frac{n}{N}\right) + \delta\omega_2\ sin\left(2\pi f_2\ \frac{n}{N}\right), \tag{6.1}$$

where we chose $f_1 = 10$ and $f_2 = 16$. The simulated eigenvalue spectrum and the JSI for this modulation pattern are also shown in Figure 6.2 .g and i. We now observe the omission of two sets of peaks, again located symmetrically around the pump frequency. This shows that our scheme to engineer spectral correlation between generated photon pairs can be extended to more complex patterns.

We note that, in addition to a targeted mode, the sinusoidal modulation pattern also shifts neighboring eigenmodes to some extent. Nevertheless, we find that such intended shifts do not affect the JSI significantly. This is because of the intrinsic (κ_{in}) and extrinsic losses (κ_{ex}) that result in a

finite width of the resonances corresponding to each eigenmode. If the shifts in eigenenergies are small compared to these linewidths, we do not expect to see a significant change in JSI.

Chapter 7

Genetic Optimization for Compensation of Fabrication Disorders

While coupled-resonator systems provide access to additional degrees of freedom to engineer the propagation of photons, applications of such large-scale arrays are hindered by fabrication disorders that lead to random variations in ring resonance frequencies. In the presence of such disorders, the mode structure of a device can be very significantly different compared to the desired spectrum, to the extent that the device might not be usable.

One solution to this problem of fabrication disorders is the use of topological features, such as edge states, to ensure that the mode structure of the coupled resonator system is robust against fabrication disorders. Indeed, the advantages of such topologically robust edge states over conventional 1D arrays (with no robustness) have been experimentally demonstrated in photonic devices fabricated using a commercial state-of-the-art fabrication process [38]. This robustness has also been used to implement topologically robust sources of quantum light and optical frequency combs [24, 27, 25].

An engineering approach to compensate for fabrication disorders is to simply tune the ring resonance frequencies after fabrication. This tuning could be achieved, for example, using thermal heaters that are fabricated over the ring resonator waveguides. The heat generated by the heaters changes the refractive index of the waveguide via the thermo-optic effect and thereby, tunes the resonance frequency of the ring. This approach has been used for coupled-resonator systems involving two or a few (˜ 10) rings.

While this approach of tuning ring resonances after fabrication is relatively straightforward,

its implementation requires a measurement of the individual ring resonance frequencies so that the required shift can be achieved with the heaters. This knowledge of individual ring resonance frequencies, in a coupled resonator system with fixed couplings, is challenging because any measurement would yield the response of the complete array. Such a measurement is also challenging because it requires access to each ring using input/output waveguides that can lead to an extra loss on each ring and could be very difficult to implement in 2D resonator arrays.

Previous implementations of thermally tuned ring resonator systems have addressed this challenge by measuring the transmission spectrum of the coupled resonator system. As we discussed earlier, the peaks (or dips) in the transmission spectrum are associated with the presence of supermode resonances in the system. Therefore, a measurement of the transmission spectrum can be used to estimate the positions of the supermode resonances (given the resonances are well resolved, which is the case with low-loss systems). However, demonstrations of this approach have been mostly limited to the system of two or only a few (~ 10) coupled resonators where a brute-force optimization of the transmission spectrum could be carried out to match it with a desired spectrum.

In this chapter, we will show that genetic optimization could be used to systematically estimate the disorder-induced shifts in resonance frequencies of a coupled resonator array. We assume that each resonator has a heater available to tune the individual resonance frequencies. We also assume that the supermode resonances are well resolved in the transmission spectrum of the coupled resonator system, that is, the total intrinsic and extrinsic loss of the array is small compared to the coupling strength. This assumption has been made to simplify the numerical simulation protocol and is also valid in many coupled resonator arrays.

The experimental protocol will involve selecting an initial population, that is, a set of resonance frequency detunings to apply on the resonators and estimating the supermode resonances via transmission measurements. The root-mean-square error in the estimated supermode resonances, compared to the simulated/desired resonances, is fed into the optimization algorithm to get a new set of populations, that is, a new set of detunings to apply on the resonators, that would lower the error. Repeating this protocol, over many generations would yield a solution, that is, a set of resonance frequency detunings for each resonator that will yield a supermode spectrum that is very close to the simulated/desired spectrum without any disorders. In the following, we will present one example of this approach using numerical simulations.

We start with a 1D resonator chain with 20 identical resonators with open boundary conditions. We generate a set of random numbers, with a normal distribution in the range $\delta\omega_0 = \pm 0.2J$, which quantifies the strength of the disorder. These random numbers correspond to the

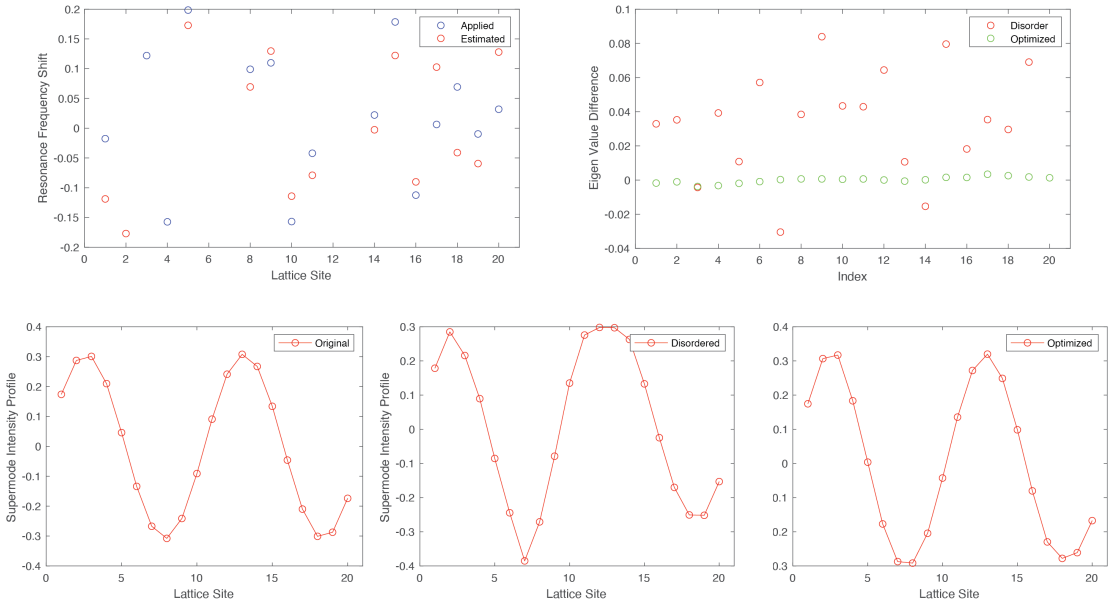


Figure 7.1: Disorder compensation for a 1D resonator chain, with OBC, using genetic optimization.

disorder in the ring resonance frequencies, that is, $\omega_0 - \omega_{0,n}$, where ω_0 is the designed resonance frequency and $\omega_{0,n}$ is the actual resonance frequency or the ring (after fabrication). In Figure 7.1, we show the generated set of random resonance frequency shifts (corresponding to inherent disorder) and compare them with the shifts estimated using genetic optimization.

Chapter 8

Conclusions and Outlook

The supermodes of coupled resonator arrays provide a versatile platform for engineering the dispersion, and therefore, propagation of photons. They have found applications such as optical delay lines and buffers, flat-top wavelength filters, quantum light sources, and so on. Nevertheless, existing approaches to designing coupled resonator arrays have been limited to simple lattices, such as 1D or 2D arrays with identical resonators. The choice of the lattice governs the resonance frequencies of the supermodes and their dispersion characteristics.

In this thesis, starting with these simple resonator geometries as a template, we explored the use of inverse design techniques to engineer their dispersion. We focused on two techniques, the intuitive Fourier-transform-based techniques that use simple sinusoidal variations of ring resonance frequencies, and the more general genetic-optimization-based techniques that go beyond intuition and fine-tune the array to achieve a desired set of supermode resonance frequencies.

For both techniques, we found that the inherent mode structure of the array plays a significant role in dictating possible supermode eigenvalue spectra. Specifically, we found that any resonance shift in a target supermode results from its coupling to neighboring supermodes. For the 1D array with OBC, this coupling was between different standing-wave type supermodes. For the 1D array with PBC, this coupling was between CW and CCW traveling-wave supermodes and was a result of the back-reflection caused by a change in the ring resonance frequencies. For the OBC, it was possible to significantly shift a single target supermode while minimizing shifts of other supermodes. For PBC, the double-degeneracy of the supermodes made it impossible to achieve a selective shift of a single target supermode - the shift was always observed in a pair of supermodes that acquire the same phase ($m\ 2\pi$) when circulating around the array.

For the 2D topological array, the supermodes of interest were the topological edge states.

However, we found that the inherent robustness of the topological edge states precludes any variations in the ring resonance frequencies to selectively shift a mode. We attempted to use back-scattering-induced coupling between CW and CCW modes of individual resonators, but such a coupling would split the degeneracy of all the edge modes and there was no selectivity.

We emphasize that while in this thesis we only presented a few examples of supermode engineering, the techniques that we explored are very general and can be used to implement a much more complex supermode spectrum in large arrays. Furthermore, while we focused on ring resonator arrays, the techniques that we have developed can be directly applied to other resonator arrays, for example, using photonic crystal cavities, microwave or superconducting resonator arrays. For simplicity, we have also focused on a single optimization algorith, the genetic optimization which has been recently used to engineer modes of single-ring resonators. Application of other optimization algorithms could achieve better or faster results.

We presented an application of supermode engineering, that is, engineering the spectral correlations between energy-time entangled photons generated via spontaneous four-wave mixing. We found that shifting the energy of a given supermode can break the energy conservation and, therefore, suppress the generation of signal/idler photons corresponding to those particular supermodes. This scheme could be extended to generate designer quantum states of light that are frequency-bin entangled, for example, in higher dimensions using supermodes of coupled resonators or continuous-variable cluster states.

We note that, in addition to a significant energy shift of only one or more target supermodes, we always observe some intended shifts in neighboring modes. These shifts could be significant or negligible depending on the technique used for their optimization and their relation with the target supermode. More importantly, we note that if such unintended shifts, in modes other than the target supermode, are smaller than the linewidth of the supermodes, they might be ignored. We saw one example of this phenomenon when calculating the joint-spectral intensity of signal-idler photon pairs. The generation of photons was suppressed only by the supermode that was shifted very significantly in energy. Photon pair generation in other supermodes that showed small shifts was not affected significantly.

In the future, we believe that this technique could be very easily extended to engineer a novel class of nonlinear optical frequency combs, called nested combs, that can be generated using coupled resonator arrays [27]. Specifically, the generation of optical frequency combs using Kerr nonlinearities is very susceptible to the dispersion of the resonators as well as that of the supermodes. By using inverse design techniques, it might be possible to specifically omit particular comb teeth

or to enhance the intensity of particular comb teeth. Such engineered nested combs could find applications in spectroscopy, on-chip microwave synthesis using photonics, LiDARs and so on.

Bibliography

[1] B. Little, S. Chu, H. Haus, J. Foresi, and J.-P. Laine, "Microring resonator channel dropping filters," *J. Light. Technol.*, vol. 15, no. 6, pp. 998–1005, Jun. 1997.

[2] Q. Xu, B. Schmidt, S. Pradhan, and M. Lipson, "Micrometre-scale silicon electro-optic modulator." *Nature*, vol. 435, no. 7040, pp. 325–7, May 2005.

[3] C. Sun, M. T. Wade, Y. Lee, J. S. Orcutt, L. Alloatti, M. S. Georgas, A. S. Waterman, J. M. Shainline, R. R. Avizienis, S. Lin, B. R. Moss, R. Kumar, F. Pavanello, A. H. Atabaki, H. M. Cook, A. J. Ou, J. C. Leu, Y.-H. Chen, K. Asanović, R. J. Ram, M. A. Popović, and V. M. Stojanović, "Single-chip microprocessor that communicates directly using light," *Nature*, vol. 528, no. 7583, pp. 534–538, Dec. 2015.

[4] H. Xu, M. Hafezi, J. Fan, J. Taylor, G. F. Strouse, and Z. Ahmed, "Ultra-sensitive chip-based photonic temperature sensor using ring resonator structures," *Optics Express*, vol. 22, no. 3, pp. 3098–3104, 2014.

[5] P. Del'Haye, A. Schliesser, O. Arcizet, T. Wilken, R. Holzwarth, and T. J. Kippenberg, "Optical frequency comb generation from a monolithic microresonator," *Nature*, vol. 450, no. 7173, pp. 1214–1217, Dec. 2007.

[6] T. J. Kippenberg, R. Holzwarth, and S. A. Diddams, "Microresonator-based optical frequency combs," *Science*, vol. 332, no. 6029, pp. 555–559, Apr. 2011.

[7] T. J. Kippenberg, A. L. Gaeta, M. Lipson, and M. L. Gorodetsky, "Dissipative kerr solitons in optical microresonators," *Science*, vol. 361, no. 6402, 2018.

[8] A. L. Gaeta, M. Lipson, and T. J. Kippenberg, "Photonic-chip-based frequency combs," *Nat. Photonics*, vol. 13, no. 3, pp. 158–169, Mar. 2019.

[9] S. Clemmen, K. P. Huy, W. Bogaerts, R. G. Baets, P. Emplit, and S. Massar, "Continuous wave photon pair generation in silicon-on-insulator waveguides and ring resonators," *Opt. Express*, vol. 17, no. 19, pp. 16 558–16 570, Sep 2009.

[10] L. G. Helt, Z. Yang, M. Liscidini, and J. E. Sipe, "Spontaneous four-wave mixing in microring resonators," *Opt. Lett.*, vol. 35, no. 18, pp. 3006–3008, Sep 2010.

[11] J. Chen, Z. H. Levine, J. Fan, and A. L. Migdall, "Frequency-bin entangled comb of photon pairs from a silicon-on-insulator micro-resonator," *Opt. Express*, vol. 19, no. 2, pp. 1470–1483, Jan 2011.

[12] A. Yariv, Y. Xu, R. K. Lee, and A. Scherer, "Coupled-resonator optical waveguide: a proposal and analysis." *Opt. Lett.*, vol. 24, no. 11, pp. 711–713, Jun. 1999.

[13] J. Poon, J. Scheuer, S. Mookherjea, G. Paloczi, Y. Huang, and A. Yariv, "Matrix analysis of microring coupled-resonator optical waveguides." *Opt. Express*, vol. 12, no. 1, pp. 90–103, Jan. 2004.

[14] S. Mookherjea, "Dispersion characteristics of coupled-resonator optical waveguides," *Opt. Lett.*, vol. 30, no. 18, pp. 2406–2408, 2005.

[15] F. Xia, L. Sekaric, and Y. Vlasov, "Ultracompact optical buffers on a silicon chip," *Nat. Photonics*, vol. 1, no. 1, pp. 65–71, Jan. 2007.

[16] A. Melloni, A. Canciamilla, C. Ferrari, F. Morichetti, L. O'Faolain, T. Krauss, R. D. L. Rue, A. Samarelli, and M. Sorel, "Tunable delay lines in silicon photonics: coupled resonators and photonic crystals, a comparison," *IEEE Photonics J.*, vol. 2, 2010.

[17] H.-C. Liu and A. Yariv, ""Ideal" optical delay lines based on tailored-coupling and reflecting, coupled-resonator optical waveguides." *Opt. Lett.*, vol. 37, no. 11, pp. 1964–6, Jun. 2012.

[18] a. Canciamilla, M. Torregiani, C. Ferrari, F. Morichetti, R. M. De La Rue, a. Samarelli, M. Sorel, and a. Melloni, "Silicon coupled-ring resonator structures for slow light applications: potential, impairments and ultimate limits," *J. Opt.*, vol. 12, no. 10, p. 104008, Oct. 2010.

[19] J. R. Ong and S. Mookherjea, "Quantum light generation on a silicon chip using waveguides and resonators," *Opt. Express*, vol. 21, no. 4, pp. 5171–5181, Feb 2013.

[20] R. Kumar, J. R. Ong, M. Savanier, and S. Mookherjea, "Controlling the spectrum of photons generated on a silicon nanophotonic chip," *Nature Communications*, vol. 5, p. 5489, 2014.

[21] M. Hafezi, E. A. Demler, M. D. Lukin, and J. M. Taylor, "Robust optical delay lines with topological protection," *Nat. Phys.*, vol. 7, no. 11, pp. 907–912, Aug. 2011.

[22] M. Hafezi, S. Mittal, J. Fan, A. Migdall, and J. M. Taylor, "Imaging topological edge states in silicon photonics," *Nature Photonics*, vol. 7, no. 12, pp. 1001–1005, Oct 2013.

[23] S. Mittal, V. V. Orre, D. Leykam, Y. D. Chong, and M. Hafezi, "Photonic anomalous quantum hall effect," *Physical review letters*, vol. 123, no. 4, p. 043201, 2019.

[24] S. Mittal, E. A. Goldschmidt, and M. Hafezi, "A topological source of quantum light," *Nature*, vol. 561, no. 7724, pp. 502–506, 2018.

[25] S. Mittal, G. Moille, K. Srinivasan, Y. K. Chembo, and M. Hafezi, "Topological frequency combs and nested temporal solitons," *Nature Physics*, vol. 17, no. 10, pp. 1169–1176, 2021.

[26] T. Dai, Y. Ao, J. Bao, J. Mao, Y. Chi, Z. Fu, Y. You, X. Chen, C. Zhai, B. Tang, Y. Yang, Z. Li, L. Yuan, F. Gao, X. Lin, M. G. Thompson, J. L. O'Brien, Y. Li, X. Hu, Q. Gong, and J. Wang, "Topologically protected quantum entanglement emitters," *Nat. Photonics*, vol. 16, no. 3, pp. 248–257, Feb. 2022.

[27] S. Mittal, V. V. Orre, E. A. Goldschmidt, and M. Hafezi, "Tunable quantum interference using a topological source of indistinguishable photon pairs," *Nat. Photonics*, vol. 15, no. 7, pp. 542–548, May 2021.

[28] E. Lucas, S. Yu, T. Briles, D. Carlson, and S. Papp, "Tailoring microcombs with inverse-designed, meta-dispersion microresonators," *arXiv preprint arXiv:2209.10294*, 2022.

[29] J. R. Stone, X. Lu, G. Moille, D. Westly, T. Rahman, and K. Srinivasan, "Wavelength-accurate nonlinear conversion through wavenumber selectivity in photonic crystal resonators," *Nature Photonics*, pp. 1–8, 2023.

[30] G. H. Ahn, K. Y. Yang, R. Trivedi, A. D. White, L. Su, J. Skarda, and J. Vučković, "Photonic inverse design of On-Chip microresonators," *ACS Photonics*, May 2022.

[31] S. Mittal, J. Fan, S. Faez, A. Migdall, J. M. Taylor, and M. Hafezi, "Topologically robust transport of photons in a synthetic gauge field," *Physical review letters*, vol. 113, no. 8, p. 087403, 2014.

[32] J. H. Holland, *Adaptation in Natural and Artificial Systems: An Introductory Analysis with Applications to Biology, Control, and Artificial Intelligence*. Cambridge, MA: MIT Press, 1992.

[33] S. Perón Santana, M. Domínguez, and O. Osenda, "Quantum state transfer performance of heisenberg spin chains with site-dependent interactions designed using a generic genetic algorithm," *arXiv preprint arXiv:2403.15909*, 2024.

[34] I. Song, Y. Lee, and M. Kwon, "Circuit-centric genetic algorithm (cga) for analog and radio-frequency circuit optimization," *arXiv preprint arXiv:2403.17938*, 2024.

[35] G. Kam and K. Chung, "Guided-mutation genetic algorithm for mobile iot network relay," *arXiv preprint arXiv:2404.01683*, 2024.

[36] J. L. O'Brien, A. Furusawa, and J. Vučković, "Photonic quantum technologies," *Nature Photon.*, vol. 3, no. 12, pp. 687–695, 2009.

[37] M. D. Eisaman, J. Fan, A. Migdall, and S. V. Polyakov, "Single-photon sources and detectors," *Review of Scientific Instruments*, vol. 82, no. 7, p. 071101, 2011.

[38] S. Mittal and et al., "Topologically robust transport of photons in a synthetic gauge field," *Phys. Rev. Lett.*, vol. 113, no. 8, p. 087403, 2014.